

## Exploring the Relationship Between *Swift* Short Gamma-Ray Burst Afterglows and their Host Galaxy Properties

CRISTIAN CASTREJON,<sup>1</sup> ANYA E. NUGENT,<sup>2</sup> WEN-FAI FONG,<sup>1</sup> GENEVIEVE SCHROEDER,<sup>3</sup> ALICIA ROUCO ESCORIAL,<sup>4</sup> AND OLIVIA GUERRA<sup>1</sup>

<sup>1</sup>Center for Interdisciplinary Exploration and Research in Astrophysics (CIERA) and Department of Physics and Astronomy, Northwestern University, Evanston, IL 60208, USA

<sup>2</sup>Center for Astrophysics — Harvard & Smithsonian, 60 Garden St. Cambridge, MA 02138, USA

<sup>3</sup>Department of Astronomy, Cornell University, Ithaca, NY 14853, USA

<sup>4</sup>European Space Agency (ESA), European Space Astronomy Centre (ESAC), Camino Bajo del Castillo s/n, 28692 Villanueva de la Cañada, Madrid, Spain

### ABSTRACT

We present a comprehensive compilation of short-duration gamma-ray burst (GRB) afterglows in the X-ray, optical, and radio bands, comprising 150 events discovered primarily by the Neil Gehrels *Swift* Observatory over 2005–2023. We pair these observations with uniformly modeled host galaxies to understand how broadband afterglow luminosities are influenced by their environmental properties. We compare the X-ray and optical afterglow luminosities at 3 hr with projected physical and host-normalized galactocentric offsets, host stellar mass, star-formation rate (SFR), specific SFR, and stellar population age. In the radio band, we explore how these environmental properties may influence afterglow detectability. We find statistical support that X-ray afterglows are brighter in galaxies with younger ages, lower masses, and higher active star formation – trends that also scale with ISM density. While we also visualize these differences for optical afterglows, the only statistically significant trend is that they are brighter in hosts with higher SFR. We further find that X-ray (radio) afterglows are more luminous (more likely to be detected) at low projected offsets. Overall, this indicates that X-ray afterglow luminosity is the most predictable indicator of host environment among the three bands. We find the afterglow luminosities of three possible merger-driven long GRBs to be unremarkable compared to the traditional short GRB population, strengthening the case that these events arise from mergers. Finally we find that the estimated on-axis afterglow luminosity of GW170817 is in the faintest  $\approx 30\%$ , aligning with its quiescent, old and massive host environment.

*Keywords:* short gamma-ray bursts, galaxies

### 1. INTRODUCTION

The relationship between properties of astrophysical transients and their host galaxies has long been leveraged to disentangle observed features that may be due to the progenitor systems from effects due to the environment. For example, Type Ia supernovae (SNe Ia), which derive from degenerate progenitors and are vital probes of the expansion rate of the Universe (Riess et al. 1998; Perlmutter et al. 1999), are observed to have brighter peak luminosities in host galaxies with higher stellar masses ( $\gtrsim 10^{10} M_{\odot}$ ), lower specific star formation rates (sSFR), and higher gas-phase metallicities than those in the low mass, high sSFR, and low metallicity hosts (Sullivan et al. 2006; Neill et al. 2009; Kelly et al. 2010; Lampeitl et al. 2010; Sullivan et al.

2010; D’Andrea et al. 2011; Gupta et al. 2011; Childress et al. 2013; Pan et al. 2014; Rigault et al. 2020). It is thought that these observed trends arise from differences in dust relations between high- and low-mass galaxies; thus, the SN luminosity versus host property trends are a result of the environment as opposed to a difference in progenitor systems (Salim et al. 2018; Brout & Scolnic 2021; Meldorf et al. 2023). Trends with transient brightness and host properties have also been observed for the long-duration  $\gamma$ -ray burst (GRB) population, which are highly energetic, jetted explosions of  $\gamma$ -ray emission that last for  $\gtrsim 2$  seconds (Norris et al. 1984; Kouveliotou et al. 1993; Dezalay et al. 1992; Lien et al. 2016) and derive from massive stars. Long GRBs are followed by multi-wavelength synchrotron ‘afterglow’ emission (e.g., Rees & Meszaros 1992) that results from the interaction

of the relativistic jet with the circumburst environment. A subset of long GRBs with detected X-ray (and often radio) afterglows, have fainter optical afterglows than expected and often evade detection. Although such long GRBs, coined “dark” (Fynbo et al. 2001), are not distinct in their intrinsic  $\gamma$ -ray properties from optically-bright GRBs (Schroeder et al. 2022), they tend to occur in hosts with higher global dust extinction and stellar masses than those with detected optical afterglows (Krühler et al. 2011; Perley et al. 2009, 2013; Schroeder et al. 2022). Just as in SNe Ia, this demonstrates that the fainter optical afterglows of dark GRBs are largely a product of their environments, as opposed to an intrinsic trait of the transient or its progenitor.

A related class of high-energy transients are short-duration GRBs (nominal durations  $\lesssim 2$  sec), the majority of which likely originate from the mergers of two neutron stars, or a neutron star and a black hole (Abbott et al. 2017; Berger 2014). The afterglows of short GRBs are  $\approx 10 - 100$  times fainter across the electromagnetic spectrum than those of long GRBs (Panaiteescu et al. 2001; Berger 2007; Nakar 2007; Kann et al. 2011). One natural explanation is that short GRBs have intrinsically lower kinetic energy scales (e.g., Panaiteescu et al. 2001), since the brightness of the afterglow scales with kinetic energy at all wavelengths (Granot & Sari 2002). Accurate inference on the kinetic energy relies on well-sampled afterglows to enable robust modeling, as well as constraints on collimation to correct from isotropic-equivalent values to the true ones (Rhoads 1999). Indeed, based on such studies for a  $\sim$ dozen short GRBs, the intrinsic, beaming-corrected kinetic energies of short GRBs are  $\approx 10^{49} - 10^{50}$  erg (Fong et al. 2015; Rouco Escorial et al. 2023a),  $\sim 1 - 2$  orders of magnitude lower than for long GRBs (e.g., Gehrels et al. 2008). However, some short GRBs have evidence for wider jets (Laskar et al. 2022; Schroeder et al. 2024, 2025; Rouco Escorial et al. 2023b), signifying larger energy scales that may not be able to explain the faintness of short GRB afterglows alone.

An additional possibility is that short GRBs arise in environments with lower circumburst densities, a parameter which also scales with afterglow brightness. Indeed, while long GRBs are generally located proximate to star formation regions within their star-forming host galaxies (Perley et al. 2013; Wang & Dai 2014; Vergani et al. 2015; Blanchard et al. 2016; Niino et al. 2017), short GRBs occur in both actively star-forming and quiescent galaxies (Leibler & Berger 2010; Nugent et al. 2022; Jeong & Im 2024) and also occur in more remote locations (Church et al. 2011; Fong & Berger 2013; Tunnicliffe et al. 2014; Fong et al. 2022; O’Connor et al.

2022). These characteristics of the short GRB population are naturally explained by their neutron star (NS) binary progenitors, which experience a combination of systemic velocities as observed with the Galactic population (Tauris et al. 2017; Vigna-Gómez et al. 2018; Andrews & Mandel 2019; Gaspari et al. 2024) and substantial delay times of  $\sim 10$ ’s of Myr to few Gyr (Nakar 2007; Berger et al. 2007; Jeong & Lee 2010; Hao & Yuan 2013; Wanderman & Piran 2015; Tauris et al. 2017; Anand et al. 2018; Andrews & Mandel 2019; Zevin et al. 2022). As a result, short GRBs arise in older stellar populations and exhibit locations more offset from star formation than long GRBs. Commensurately, short GRBs have lower circumburst densities ( $10^{-3} - 10^{-2}$  cm $^{-3}$ ; Soderberg et al. 2006b; Fong et al. 2015; O’Connor et al. 2020; Rouco Escorial et al. 2023b) than long GRBs ( $\approx 0.1 - 100$  cm $^{-3}$ ; Schneider et al. 2022; Yost et al. 2003; Chrimes et al. 2022). A recent study showed that the small but growing population of short GRBs with radio afterglow detections have larger inferred densities than those without detections (Schroeder et al. 2025). Taken together, density very likely plays a role in the observed afterglow luminosity differences between long and short GRBs (e.g., Perna & Belczynski 2002).

However, the trends between afterglow brightness with kinetic energy and densities are based on subsets of the population with relevant data, and inferred values for these parameters are subject to modeling differences. This has motivated studies which rely on observed, as opposed to inferred, properties for larger numbers of short GRBs. For instance, O’Connor et al. (2022) investigated the ratio of X-ray flux to  $\gamma$ -ray fluence (a proxy for density if the cooling frequency is above the X-ray band; Granot & Sari 2002) versus projected galactocentric offset for a few dozen events and did not find any clear trends. In the radio band, short GRBs with radio afterglow detections tend to have smaller offsets than those which evade detection, although statistical significance in this trend has not been established (Schroeder et al. 2025). Finally, Nugent et al. 2022 found that short GRB optical afterglows may be brighter in galaxies with higher active star formation (which, at a basic level, correlates with ISM density). However, the visible trend was also not statistically significant.

A natural extension of these studies are to investigate the relationship between afterglow brightness and any host galaxy property (e.g., star formation rate, stellar mass, stellar population age, dust extinction), which will give deeper insight into how much environment plays a role in afterglow luminosity. However, this is challenging to conduct in a uniform way. First, the relatively low afterglow detection rates, particularly in the optical and

radio bands, mean that a large number of upper limits need to be accounted for in any statistical study. Second, the diversity of sampling in light curves (with some having only one data point, and some having many), coupled with the rapid fading behavior, makes interpolation to a common time highly nuanced. Finally, until recently, a homogeneous set of short GRB host galaxy properties, including those events which lacked precise (sub-arcsecond) localization, did not exist.

Here, we attempt to overcome these challenges and leverage the first substantial and uniformly-modeled samples of host galaxies, combined with two decades of short GRB afterglow observations across the electromagnetic spectrum. We analyze a population of 150 GRBs detected with the Neil Gehrels *Swift* Observatory (*Swift*) to investigate possible relations between X-ray, optical and radio afterglows to their host galaxy properties. In Section 2, we describe our sample and identify the number of events with reported X-ray, optical, and radio afterglow data, host galaxy associations, redshifts, and host stellar population properties. In Section 3, we detail our method to determine afterglow luminosity at a specified common rest-frame time. In Section 4, we investigate trends in the luminosities of X-ray and optical afterglows, as well as the detectability of radio afterglows, to environmental properties. We discuss implications for these findings and relate them to afterglow properties of long GRBs and gravitational wave events with NS merger origins in Section 5. Finally, we list our main conclusions in Section 6.

Unless otherwise stated, all observations are reported in the AB magnitude system and have been corrected for Galactic extinction in the direction of the GRB (Cardelli et al. 1989; Schlafly & Finkbeiner 2011). We employ a standard WMAP9 cosmology of  $H_0 = 69.6 \text{ km s}^{-1} \text{ Mpc}^{-1}$ ,  $\Omega_m = 0.286$ ,  $\Omega_{\text{vac}} = 0.714$  (Hinshaw et al. 2013; Bennett et al. 2014).

## 2. GRB SAMPLE

We begin with the sample of all short GRBs detected by *Swift* (Gehrels et al. 2004) with  $T_{90} < 2$  seconds (excluding GRB 170817A), and those that have been classified as having extended emission (Lien et al. 2016). We exclude any short GRBs that derive from collapsar origins (GRBs 080913, 090423, 100724A, and 200826A; Zhang et al. 2009; Ahumada et al. 2021; Rhodes et al. 2021; Zhang et al. 2021), as these likely do not share the same origin as the rest of the short GRB population. This comprises 150 GRBs that were observed and localized between February 2005 and November 2023 (ending with GRB 231117A). Since our study hinges upon correlations with afterglow brightness, we trim the sample to

only include those with any afterglow follow-up observations. This comprises 105 short GRB events in the X-ray band, 132 in the optical band, and 86 in the radio band. We also include three long GRBs: GRBs 060614 (Jin et al. 2015; Yang et al. 2015; Gompertz et al. 2018; Rossi et al. 2020), 211211A (Rastinejad et al. 2022a; Troja et al. 2022; Yang et al. 2022), and 230307A (Gillanders et al. 2023; Levan et al. 2024; Yang et al. 2024). Despite their long durations, these events are associated with probable  $r$ -process kilonovae (KN), indicative of NS merger origins. All have reported X-ray, optical, and radio afterglows. Thus, in total we consider 108 events with X-ray, 135 with optical, and 89 with radio observations. The summary of our sample, split by availability of observations within each wavelength, is depicted in Figure 1 and listed in Table A1.

We collect all X-ray afterglow data from the *Swift* light-curve repository (Evans et al. 2007, 2009), supplemented by *Chandra* and XMM-Newton data reported in Rouco Escorial et al. (2023a) and references therein. We collect optical afterglow data for 111 GRBs from Fong et al. (2015), Rastinejad et al. (2021c), and references therein. For an additional 24 GRBs, we collect optical afterglow data from the Gamma-ray Coordination Network (GCN) stream and the literature. Of the bursts with optical data, we exclude five events that do not have any data in one of the  $grizV$ -bands. We find available radio afterglow data for 89 short GRBs within various GCNs and publications (see Table A1 for references). Of the 89 in the radio band, 24 have shallow radio observations of  $\gtrsim 100 \mu\text{Jy}$  (Chastain et al. 2024; Schroeder et al. 2025) resulting in non-detections; we do not include these GRBs in our sample of upper limits since we do not have meaningful constraints on their non-detection (see Table A1). The full list of references for our afterglow data is in Table A1.

In addition to the afterglow data, we also require a host galaxy association for inclusion in the sample as our study is focused on correlations to host properties. All host associations, galactocentric offsets, redshifts, and host stellar population properties were obtained from the Broadband Repository for Investigating Gamma-ray burst Host Traits (BRIGHT<sup>1</sup>; Fong et al. 2022; Nugent et al. 2022) and from Levan et al. (2024); Schroeder et al. (2025); Nugent et al. (2025).

In Figure 1, we display the total sample, categorized by their detectability in each wavelength. We further list the sample sizes for the subsets of bursts that have specific environmental properties. We show the X-ray

<sup>1</sup> <http://bright.ciera.northwestern.edu>

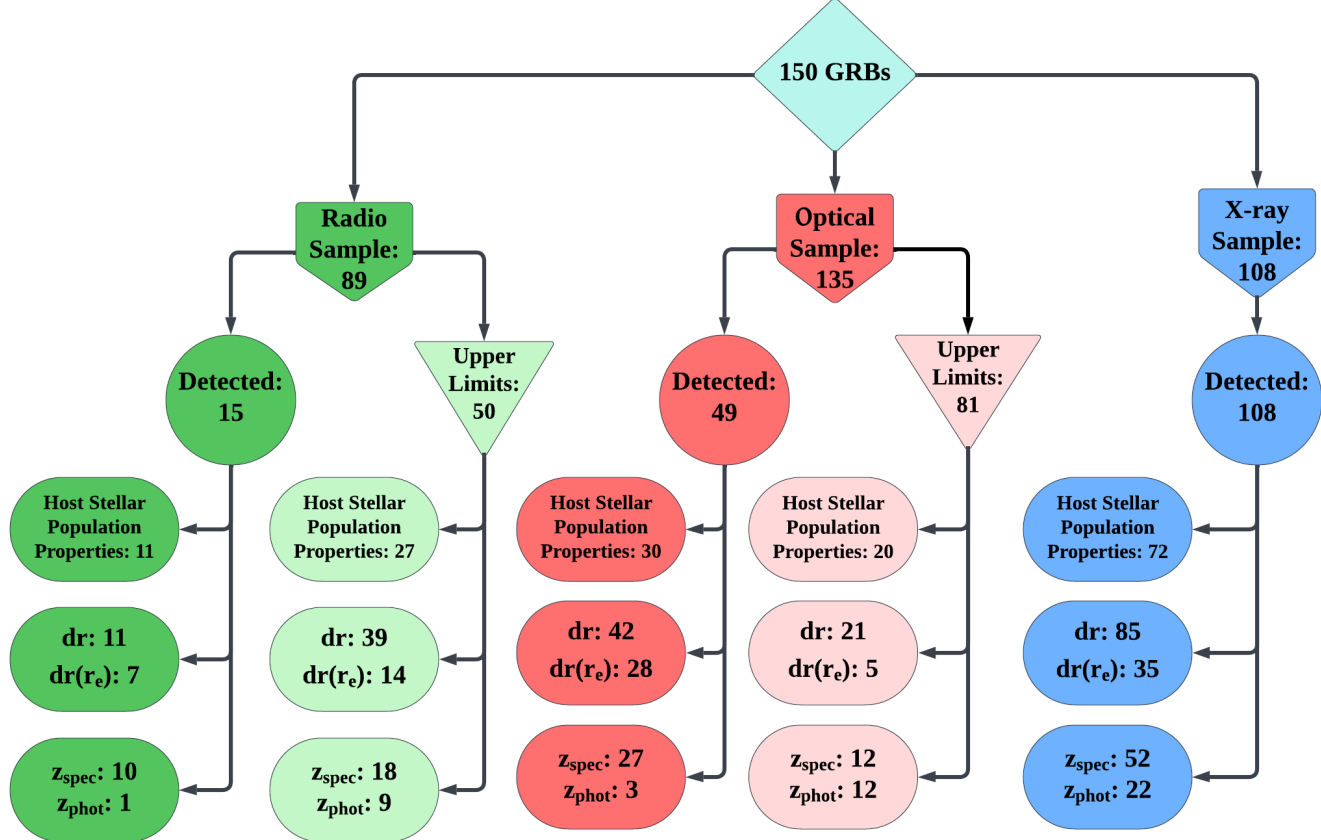


**Figure 1.** A flowchart depicting the breakdown of our sample at each wavelength (X-ray: blue, optical: red, and radio: green). Within each wavelength, we display the number of GRBs that have either detected afterglows or upper limits. We further include the number of GRBs that have host stellar populations, physical and host-normalized offsets, and spectroscopic versus photometric redshifts. We note that five GRBs have no *griz* or *V*-band filters available, and thus appear in the second row but not the third. Similarly, 24 GRBs with only shallow radio limits ( $> 100 \mu\text{Jy}$ ) and otherwise no detections and are not considered in our radio upper limits.

and optical afterglow light curves of all events with detections and upper limits in Figure 2 (see Section 3). In Table A1, we list the  $\gamma$ -ray T<sub>90</sub> for each GRB and whether it has available X-ray, optical, and radio afterglow data (upper limits or detections). In total, we have collected 3812 X-ray detections, 1412 optical detections and upper limits, and 253 radio detections and upper limits. Our short GRB sample further spans a wide range of redshifts:  $0.01 < z < 2.79$ . This dataset is the largest collection of short GRB afterglows to-date.

### 3. METHODS

We seek to investigate whether short GRB afterglow luminosities are correlated with any environmental property, including the short GRB galactocentric offsets and their host galaxy stellar population properties. Given that our sample spans a wide range of redshifts (Section 2) and that afterglows fade rapidly, it is important to determine the afterglow luminosities ( $L_c$ ) at a single

common rest-frame time ( $\delta t_c$ ) (D’Avanzo et al. 2012). In the following subsections, we describe our methods for computing  $L_c$  from the observed X-ray and optical afterglows. Owed to the very sparse sampling of radio afterglows, and the fact that radio afterglows rise at later times (Granot & Sari 2002), precluding simple interpolations, we do not calculate  $L_c$  for radio afterglows. We do, however, present results based on whether or not a radio afterglow is detected (Section 4).

#### 3.1. Deriving X-ray Luminosities at a Common Time

In the X-rays, we first convert the afterglow fluxes to luminosities given the redshifts of each short GRB<sup>2</sup>. We then convert all observed afterglow times to the rest-frame to luminosities given the redshifts of each short GRB (Table B2). In cases in which the redshift is not

<sup>2</sup> Since the majority of our sample has X-ray detections, we do not use X-ray afterglow upper limits in this analysis.

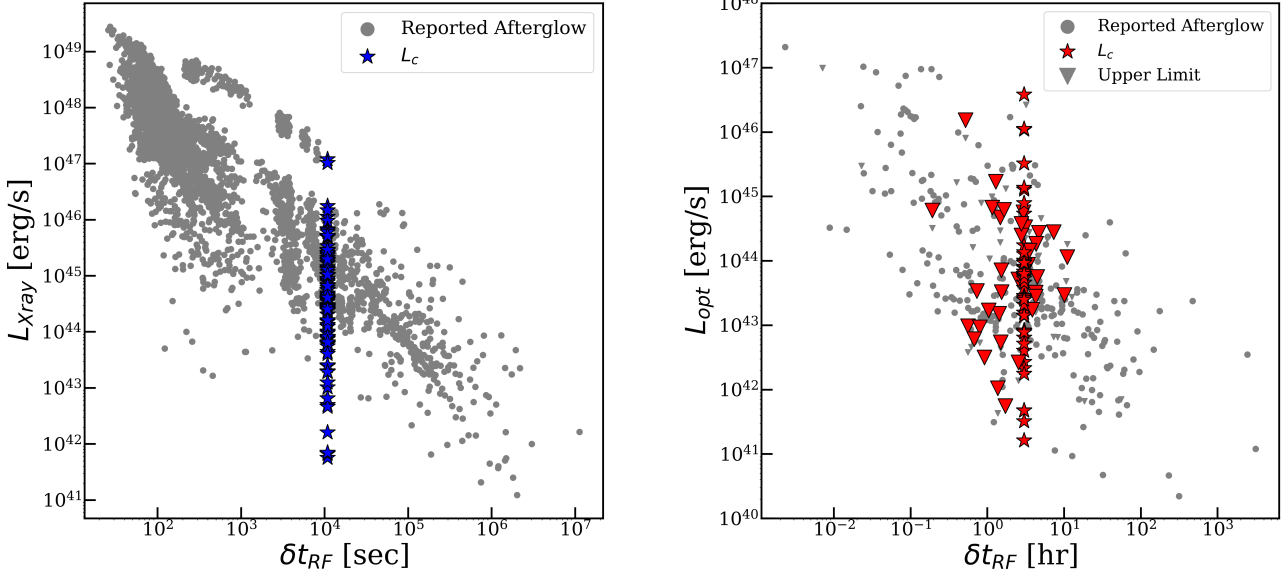


**Figure 2.** *Left:* The detected X-ray afterglow luminosities compared to rest-frame time after the burst ( $\delta t_{RF}$  for our short GRB sample (gray circles). The blue stars represent the luminosity determined at a common rest-frame time ( $L_c$ ) of 3 hr, following the methods described in Section 3. *Right:* The detected optical afterglows (gray circles) and upper limits (gray triangles) for our short GRB sample. The red stars show the  $L_c$  determined at 3 hr and the red triangles show the GRBs with reported upper limits at  $\delta t_{RF} \pm 2.8$  hr which we use in our study.

known, we use the median redshift of the sample determined of  $z \approx 0.64$  (Fong et al. 2022; Nugent et al. 2022) for these conversions. We consider two different scenarios to determine  $L_c$  depending on the amount of available data we have: (i) there exists  $> 1$  detection at  $\delta t_c \pm 2.83$  hr<sup>3</sup>, or (ii) there are  $\leq 1$  detections at  $\delta t_c \pm 2.83$  hr. Hereafter, we adopt a value of  $\delta t_c = 3$  hr, given that the majority of GRBs (71%) have X-ray afterglow data observed within 2.83 hr of the  $\delta t_c$ . We also perform the same analysis at  $\delta t_c = 10$  hr which significantly trims the sample; in Section 4, we comment on how our results are generally not sensitive to our choice.

To determine  $L_c$  for scenario (i), we use `interp1d` from the Python package `scipy` to interpolate over the available luminosity values that fall within  $\delta t_c \pm 2.83$  hr. We require that there exist at least one detection each, prior to and after  $\delta t_c$ , for proper interpolation. Furthermore, we do not include any X-ray data immediately following the burst ( $\delta t \lesssim 10$  sec) as this often considered a feature from the burst itself rather than real afterglow (Nousek et al. 2006; D’Avanzo et al. 2012). We find that 55 GRBs fit the criteria for scenario (i). To determine

uncertainties on  $L_c$ , we take all available X-ray data and find that the median uncertainty is  $\sigma_{L_X}/L_X \approx 0.2$ ; thus, we adopt 20% of each  $L_c$  as the fiducial uncertainty.

For scenario (ii) ( $\leq 1$  detections at  $\delta t_c \pm 2.83$  hr), we find that 53 GRBs fall in this category. For the GRBs with only one detection within 2.83 hr of  $\delta t_c$ , we take that detection and extrapolate to  $\delta t_c = 3$  hr, using a single power-law with  $L_X \propto t^{-1}$  to calculate  $L_c$ . We employ a power-law index of  $-1$  as this characterizes the median afterglow decline rate for short GRBs with well-sampled afterglows (Margutti et al. 2013; Fong et al. 2015; Rouco Escorial et al. 2023b). As with scenario (i), we adopt  $\sigma_{L_c} = 0.2L_c$  as the uncertainty on  $L_c$ . For events with no detections within  $\delta t_c \pm 2.83$  hr, we use the nearest (in time) data point outside of this time interval, and perform the same extrapolation using  $L_X \propto t^{-1}$ . Of the 53 GRBs that fall in scenario (ii), only 14 are in this sub-category. We highlight the observed X-ray lightcurves and  $L_X$  determined at  $t_c = 3$  hours in Figure 2.

### 3.2. Deriving Optical Luminosities at a Common Time

There are a few key differences between optical and X-ray afterglow observations for short GRBs that require modification of our techniques for determining  $L_c$ . For example, KNe are an additional source of emission that can affect the behavior of optical afterglows and some-

<sup>3</sup> We find that this time interval is large enough so it includes enough data for accurate interpolation (which requires at least two data points) but small enough that it mitigates the effects of temporal breaks (e.g., Rhoads 1999).

times dominate the light at a given time or wavelength. For the 12 GRBs that have possible KNe<sup>4</sup> we determine which detections are strongly contaminated by KN light based on published data (Berger et al. 2013a; Tanvir et al. 2013; Jin et al. 2015; Yang et al. 2015; Fong et al. 2016; Jin et al. 2016; Kasliwal et al. 2017; Gompertz et al. 2018; Troja et al. 2018a; Rossi et al. 2020; Fong et al. 2021; Rastinejad et al. 2021c; O'Connor et al. 2022; Troja et al. 2022; Yang et al. 2022; Gillanders et al. 2023; Zhou et al. 2023; Levan et al. 2024; Yang et al. 2024), and exclude all such data from our calculation of  $L_c$ . For GRBs 050709 and 070809, if they truly have KNe, then all of the available optical data would be KN-dominated. However, the luminosities of the early-time points are also consistent with afterglow emission and their identification as KNe are less certain; thus, we only use the earliest observations for these two events. For GRB 211211A, there is a well-sampled light curve with the contributions of the afterglow and kilonova determined self-consistently in Rastinejad et al. (2025). Thus, we use the afterglow contribution at  $\delta t_c$  for this event. For GRB 230307A, we use optical afterglow observations at  $\delta t < 24$  hr only, as observations beyond this clearly deviate from the afterglow models (Rastinejad et al. 2025; Yang et al. 2024). We mention the KN-dominated times ranges for these 12 events at the end of Table A1.

As optical afterglow luminosity not only changes as a function of time, but also wavelength, we prioritize minimizing the number of filters used to derive  $L_c$ . Since the majority of our sample and environmental properties are  $r$ -band observations (52%; including  $r'$ ,  $R$ ,  $R_c$ , and  $F606W$ ), we select this as the default filter. If no  $r$ -band data is available, we then prioritize the filters in the order of:  $i$  (incl.  $i'$ ,  $I$ ,  $I'$ ,  $Ic$ ; 21%),  $g$  (incl.  $g'$ ; 11%),  $z$  (incl.  $z'$ ; 4%), and  $V$  (12%). We correct all optical afterglow magnitudes for Galactic extinction in the direction of each burst and host galaxy extinction ( $A_V$ ) if known; the results are in Table B2.

After making a filter selection, we convert the optical afterglow light curves to rest-frame time and luminosities, using the same redshift considerations as we did for the X-rays (Section 3.1). To compute  $L_c$ , we again employ different methods based on the number of single-filter optical afterglow detections that exist: there are (i)  $\geq 2$  detections, (ii) 1 detection, or (iii) no detections (only upper limits). We choose  $\delta t_c = 3$  hr, given that most upper limits, which cannot be interpolated, are

near this time. Further,  $\sim 55\%$  of GRBs with  $r$ -band data fall within  $\delta t_c \pm 2.5$  hr. To address any potential bias in our conclusions by using  $\delta t_c = 3$  hr, we also perform an analysis at a later time of  $\delta t_c = 10$  hr, using the same methods to determine  $L_c$  as described here. The majority of our conclusions remain when using either of these  $\delta t_c$  and we point the reader to Section 4 for more details.

We determine the  $L_c$  for scenario (i), when there are  $\geq 2$  detections, by fitting the luminosities and rest-frame times with a power law in linear space, with the form:  $L = n \times t^\alpha$ . We employ the `curve_fit` function from `scipy` to determine the optimal values for  $n$  and  $\alpha$ , which uses a non-linear least-squares to fit the detected luminosity points to the power law. We then calculate  $L_c$  using the optimal  $n$  and  $\alpha$ . There are 34 GRBs that fit the criteria for this scenario. In the case when there are more than two data points, we calculate  $\sigma_{L_c}$  using the estimated approximate covariance matrix output from the `curve_fit` function. This applies to 21 out of the 34 GRBs. In cases where there are only two data points, preventing an accurate error on  $L_c$ , we instead use  $\sigma_{L_c} = 0.15L_c$  (the median optical afterglow luminosity error).

For scenario (ii), when there is only a single detection (14 GRBs), we use a single  $L_{\text{opt}} \propto t^{-1}$  power law to calculate the  $L_c$  instead relative to the detection. We calculate  $\sigma_{L_c}$  using the median optical afterglow luminosity error,  $\sigma_{L_c} = 0.15L_c$ . Finally, for scenario (iii), when there are only upper limits (36 GRBs), we simply use the deepest upper limit at  $\delta t_c \pm 2.5$  hr for a limit  $L_c$ , as this is the most stringent observational constraint on the GRB afterglow.

## 4. RESULTS

Equipped with the afterglow luminosities at a common time ( $L_c$ ) in both the X-ray and optical bands, we next compare these values to host environmental properties. We explore the following properties: galactocentric offsets (physical:  $\delta R_{\text{phys}}$  and host-normalized:  $\delta R_{\text{norm}}$ ), stellar mass ( $M_*$ ), star formation rate (SFR), specific star formation rate (sSFR), and mass-weighted stellar population age ( $t_m$ ). For the radio afterglows, which lack well-sampled light curves from which to extract such luminosities, we instead investigate trends between the detection (or non-detection) of a radio afterglow and any environmental properties.

### 4.1. Physical Offsets

We first consider afterglow luminosity and projected galactocentric offsets in physical units ( $\delta R_{\text{phys}}$ ). Since

<sup>4</sup> These are GRBs 050709, 050724A, 060614, 070714B, 070809, 080503, 130603B, 150101B, 160821B, 200522A, 211211A, and 230307A.

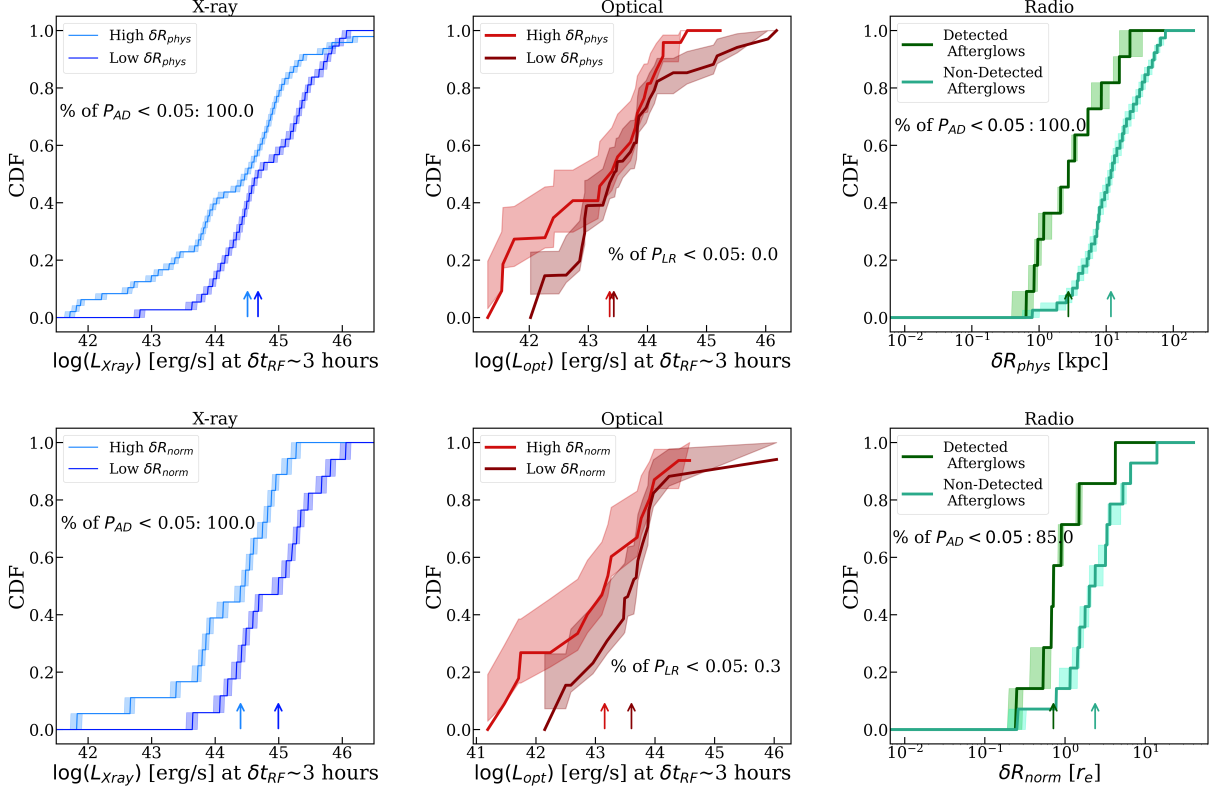


**Figure 3.** *Left Column:* CDFs of the X-ray afterglows of short GRBs at  $\delta t_c = 3$  hr with  $\delta R_{\text{phys}} > 7$  kpc or  $\delta R_{\text{norm}} > 1.66 r_e$  (light blue), and  $< 7$  kpc or  $< 1.66 r_e$  (dark blue). The median in each distribution is represented by a color-coded arrow denoted from the legend. *Middle Column:* CDFs of the optical afterglows of short GRBs at  $\delta t_c = 3$  hr with  $\delta R_{\text{phys}} > 7$  kpc or  $\delta R_{\text{norm}} > 1.66 r_e$  (light red) and  $< 7$  kpc or  $< 1.66 r_e$  (dark red). The median in each distribution is represented by a color-coded arrow denoted from the legend. *Right Column:* CDFs of the  $\delta R_{\text{phys}}$  or  $\delta R_{\text{norm}}$  for short GRBs with detected radio afterglows (dark green) versus only upper limits (light green) with arrows pointing at the median. We compare all distributions through AD (X-ray and radio) or logrank (optical) tests. For X-ray optical, and radio afterglows, we show the percentage of tests that reject the null hypothesis. We find that short GRBs with smaller  $\delta R_{\text{phys}}$  and  $\delta R_{\text{norm}}$  have brighter X-ray afterglows. In addition, short GRBs with detected radio afterglows tend to have smaller  $\delta R_{\text{phys}}$ .

the density of the ISM in galaxies generally decreases with increasing radial offset (Bigiel & Blitz 2012; Wang et al. 2014; Casasola et al. 2017; van der Giessen et al. 2024), and the afterglow brightness scales with circumburst density depending on the observing band (Granot & Sari 2002), we naively expect brighter afterglows at smaller offsets<sup>5</sup> (see Section 5). To explore a potential correlation, we divide our population into low-offset ( $\delta R_{\text{phys}} < 7$  kpc) and high-offset ( $\delta R_{\text{phys}} > 7$  kpc) events, where  $\sim 7$  kpc is the median projected offset for short GRBs (Fong et al. 2022). For each GRB, we create a probability density function (PDF) for its  $L_c$  value, assuming Gaussian uncertainties. We then generate 1000 random draws from each of the  $L_c$  PDFs, and build cumulative distribution functions (CDFs) in

luminosity for the low- and high-offset populations. We show the X-ray luminosity CDFs in Figure 3, and list the luminosity population medians and 68% confidence intervals in Table 1 (along with all other environmental properties studied in this section). As expected, the low-offset events have overall brighter X-ray afterglows than the high-offset events.

For a quantitative comparison, we perform an Anderson Darling (AD) test with the null hypothesis that the distribution of afterglow luminosities at low- and high-offset populations are derived from the same underlying distribution. We compute a  $p$ -value ( $p_{AD}$ ) for each of the 1000 distributions. If  $\geq 50\%$  of the 1000  $p$ -values are  $p_{AD} < 0.05$ , we can reject the null hypothesis that the populations derive from the same underlying distribution. For the X-ray band, we find that  $p_{AD} < 0.05$  for 100% of the draws, demonstrating a strong rejection of the null hypothesis. This indicates that the low- and high-offset distributions are statistically distinct in their

<sup>5</sup> We note that we can only measure projected offset, so any possible trend may not be very strong.

**Table 1.** Split  $L_c$  Distribution Medians and 68% Confidence Intervals

Environmental Property	$\log(L_c)$	X-ray [erg/s]	$\log(L_c)$	Optical [erg/s]
$\delta R_{\text{phys}} > 7 \text{ kpc}$		$44.48^{+0.66}_{-1.36}$	$43.79^{+0.81}_{-1.46}$	
$\delta R_{\text{phys}} < 7 \text{ kpc}$		$44.68^{+0.89}_{-0.63}$	$43.55^{+1.16}_{-0.68}$	
$\delta R_{\text{norm}} > 1.66 r_e$		$44.44^{+0.49}_{-0.96}$	$43.17^{+0.82}_{-1.49}$	
$\delta R_{\text{norm}} < 1.66 r_e$		$44.98^{+0.64}_{-0.76}$	$43.71^{+0.32}_{-1.07}$	
$\text{SFR} > 1 M_\odot \text{ yr}^{-1}$		$44.74^{+0.64}_{-0.91}$	$43.98^{+0.77}_{-0.65}$	
$\text{SFR} < 1 M_\odot \text{ yr}^{-1}$		$44.29^{+0.85}_{-1.13}$	$42.96^{+1.01}_{-1.16}$	
$\text{sSFR} > 10^{-10} \text{ yr}^{-1}$		$44.70^{+0.70}_{-0.82}$	$43.88^{+0.87}_{-0.92}$	
$\text{sSFR} < 10^{-10} \text{ yr}^{-1}$		$44.19^{+0.80}_{-2.07}$	$43.22^{+0.87}_{-0.79}$	
$\log(M_*/M_\odot) > 9.7$		$44.14^{+1.29}_{-1.31}$	$43.65^{+1.08}_{-1.23}$	
$\log(M_*/M_\odot) < 9.7$		$44.62^{+0.62}_{-0.70}$	$43.81^{+0.86}_{-0.93}$	
$t_m > 0.8 \text{ Gyr}$		$44.11^{+0.84}_{-1.32}$	$43.83^{+0.95}_{-1.45}$	
$t_m < 0.8 \text{ Gyr}$		$44.75^{+0.76}_{-0.81}$	$43.57^{+0.87}_{-0.84}$	

NOTE—A table displaying the medians and 68% confidence intervals of the distribution of luminosities at a common rest-frame time ( $L_c$ ) split by the median environmental property. All medians reported in the X-ray band are calculated from detected afterglows, and the medians reported for optical bands are determined from both detected and non-detected afterglows.

X-ray afterglow luminosities, with low-offset events having brighter afterglows. As mentioned in Section 3, we perform the same test at  $\delta t_c = 10$  hr to determine if any correlations still hold. We find the difference in afterglow luminosities is still statistically significant at this new common time, validating this observed trend.

In the optical band, we use survival statistics to incorporate the numerous upper limits, and build the CDFs. Specifically, we use a Kaplan–Meier estimator, a non-parametric method that estimates the CDF (survival function). Here, the weight of each upper limit is distributed uniformly with the detections at lower luminosities. Similar to our treatment of X-ray afterglows, we build 1000 distributions with the Kaplan Meier estimator, incorporating each of the random draws of the detected points. Figure 3 shows that, just like the X-ray afterglows, the low-offset events appear to have brighter optical afterglows, also suggested by the population medians (Table 1). However, there is significant overlap in

the high- and low-offset distributions. To quantitatively compare the optical afterglow distributions with upper limits, we employ a Wilcoxon rank-sum test (hereafter, logrank) using the Python `lifelines/logrank` function (Davidson-Pilon 2019). This statistical test considers the survival of the upper limits, using a Wilcoxon weight and mitigates the influence of upper limits by weighing detected luminosity values more heavily. As with the AD test, we reject the null hypothesis if the majority of the logrank  $p$ -values are  $p_{\text{LR}} < 0.05$ . From the 1000 logrank tests, we find that 0% of  $p_{\text{LR}} < 0.05$ . Thus, despite the apparent differences, we find no statistical support for a difference in the low- and high-offset optical afterglow luminosities. We note that upper limits comprise  $\approx 1/3$  of the optical afterglows with offset measurements, and thus their incorporation may make the claim of statistical significance more challenging. To investigate this, we repeat the same analysis with optical afterglow detections only, but recover the same results, signifying that the inclusion of upper limits does not change the results. We also find the same result when performing this test at  $\delta t_c = 10$  hr.

For radio afterglows, we take a different approach, dividing the population into those with radio afterglow detections (11 events), and those with only upper limits (39 events). For each GRB in both distributions, we create a probability density function (PDF) for its  $\delta R_{\text{phys}}$  with its corresponding uncertainty (Fong et al. 2022). We then generate 1000 random draws from each of the  $\delta R_{\text{phys}}$  PDFs, and build cumulative distribution functions (CDFs) in  $\delta R_{\text{phys}}$  for the detected and non-detected radio afterglow populations. We show these CDFs in Figure 3 and find that those with detections have smaller offsets (medians and 68% uncertainties of  $2.7^{+12.8}_{-1.9}$  kpc for detections, and  $11.8^{+27.1}_{-7.5}$  kpc for non-detections). Here, we find that  $p_{\text{AD}} < 0.05$  for 100% of the draws, demonstrating a strong rejection of the null hypothesis. This indicates that the detected and non-detected radio afterglows distributions are statistically distinct in their projected physical offsets. Overall, we find that low-offset short GRBs have a higher chance of having a detected radio afterglow. This is consistent with the expected higher ISM densities toward the centers of galaxies, and the strong radio afterglow luminosity dependence on density (Granot & Sari 2002). It also reaffirms the results based on short GRB radio afterglows in Schroeder et al. (2025). We place all results of our statistical tests in Table 2 for  $\delta R_{\text{phys}}$  and all other environmental properties discussed in the following subsections.

## 4.2. Host-Normalized Offsets

**Table 2.** Afterglow and Environmental Property Distribution Comparisons

Wavelength	Test	$\delta R_{\text{phys}}$	$\delta R_{\text{norm}}$	SFR	$\log(\text{sSFR})$	$\log(\text{Stellar Mass})$	$t_m$
		[kpc]	[ $r_e$ ]	[ $M_\odot \text{ yr}^{-1}$ ]	[ $\text{yr}^{-1}$ ]	[ $M_*/M_\odot$ ]	[Gyr]
X-ray	<code>anderson-ksamp</code>	100%	100%	59.9%	96.7%	95.9%	100%
Optical	<code>logrank</code>	0.0%	0.3%	100%	1.2%	0.0%	0.0%
Radio	<code>anderson-ksamp</code>	100%	84.9%	0.76%	0.08%	0.0%	0.04%

NOTE—The percentage of  $p$ -values that are  $< 0.05$ , determined either from an AD (X-ray, radio) or logrank (optical) test. For X-ray and optical afterglows, we separate the sample at or near the population median of the given environmental property. For radio afterglows, we display the percentage of  $p_{\text{AD}} < 0.05$ , which we use to determine if short GRBs with radio afterglow detections have different environmental properties to those with only upper limits.

We next compare afterglows to the host-normalized offset ( $\delta R_{\text{norm}}$ ). As we have shown that afterglows tend to be more luminous at lower physical offset (Section 4.1), we can extend this expectation to host-normalized offset as well. To investigate this, we divide our population at the median  $\delta R_{\text{norm}} = 1.66 r_e$  (Fong et al. 2022) and build 1000 CDFs in the same manner as described in Section 4.1. As expected, we find that the low-offset events have overall brighter X-ray afterglows than the high-offset ones (Figure 3), with 100% of the  $p_{\text{AD}} < 0.05$ , rejecting the null hypothesis that the two distributions are drawn from the same underlying distribution. The distributions remain distinct, with statistical backing, when performing the same analysis at  $\delta t_c = 10$  hr. This fully supports our physical offset results in the X-ray band.

In the optical band, the low-offset events appear to have brighter optical afterglows than the high-offset ones, with slightly less overlap in distributions than the physical offset CDFs (Figure 3). However, this apparent difference is not statistically supported: when performing a logrank test between the distributions, we find that 0.3% of  $p_{\text{LR}} < 0.05$ , failing to reject the null hypothesis that they are drawn from the same underlying survival distribution. This lack of statistical distinction between optical afterglow luminosity and  $\delta R_{\text{norm}}$  remains at  $\delta t_c = 10$  hr, and with detections-only.

In the radio band, of the events with host-normalized offset measurements, 7 events have detections while 14 have upper limits. We find that the median offset for bursts with radio detections is smaller ( $0.7^{+1.0}_{-0.4} r_e$ ), than that of non-detections ( $2.0^{+3.6}_{-1.1} r_e$ ). This difference is statistically significant (85% of  $p$ -values have  $p_{\text{AD}} \leq 0.05$ ), with radio afterglow events being more detectable at lower host-normalized offsets.

Thus, overall we find that short GRBs have more luminous afterglows at smaller offsets across all wavelengths than those at larger offsets. However, we find that the

difference is only statistically significant in the X-ray and radio bands.

#### 4.3. Star-Formation Rate and Specific Star-Formation Rate

We next compare afterglows to host galaxy star-formation rates (SFR) and specific SFR (sSFR, defined as  $\text{SFR}/M_*$ ). In general, we expect hosts with larger SFR or sSFR values to have higher average ISM densities, leading to more luminous afterglows. We divide our sample into low SFR ( $< 1 M_\odot \text{ yr}^{-1}$ ) and high SFR ( $> 1 M_\odot \text{ yr}^{-1}$ ) hosts. Separately, we divide the population into low sSFR ( $< 10^{-10} \text{ yr}^{-1}$ ) and high sSFR ( $> 10^{-10} \text{ yr}^{-1}$ ) distributions<sup>6</sup>. Both of the SFR and sSFR thresholds were chosen to roughly align with the median values for the population (Nugent et al. 2022).

In the X-ray band, we show the distribution of CDFs in Figure 4. The events in high SFR or sSFR hosts appear to have brighter X-ray afterglows than the low SFR or sSFR distributions. For SFR, when comparing the two distributions using an AD test, we find that 60% of  $p_{\text{AD}} < 0.05$ . Thus, we reject the null hypothesis that the two distributions are drawn from the same underlying one. Additionally, we find that the difference is also statistically significant for the sSFR distributions: 100% of  $p_{\text{AD}} < 0.05$ , and thus we reject the null hypothesis that short GRBs in hosts with high and low sSFR follow the same afterglow luminosity distribution. In other words, we find that short GRB X-ray afterglows tend to be brighter in host galaxies with higher SFR or sSFR. Although we find a correlation between short GRB X-ray afterglow and SFR and sSFR at  $\delta t_c = 3$  hr, this does not hold at  $\delta t_c = 10$  hr, likely due to the decreased sample size at 10 hr.

<sup>6</sup> As sSFR is defined as  $\text{SFR}/M_*$ , higher sSFR is derived from either a host galaxy with higher SFR or with smaller  $M_*$ , or a combination of both and vice versa.

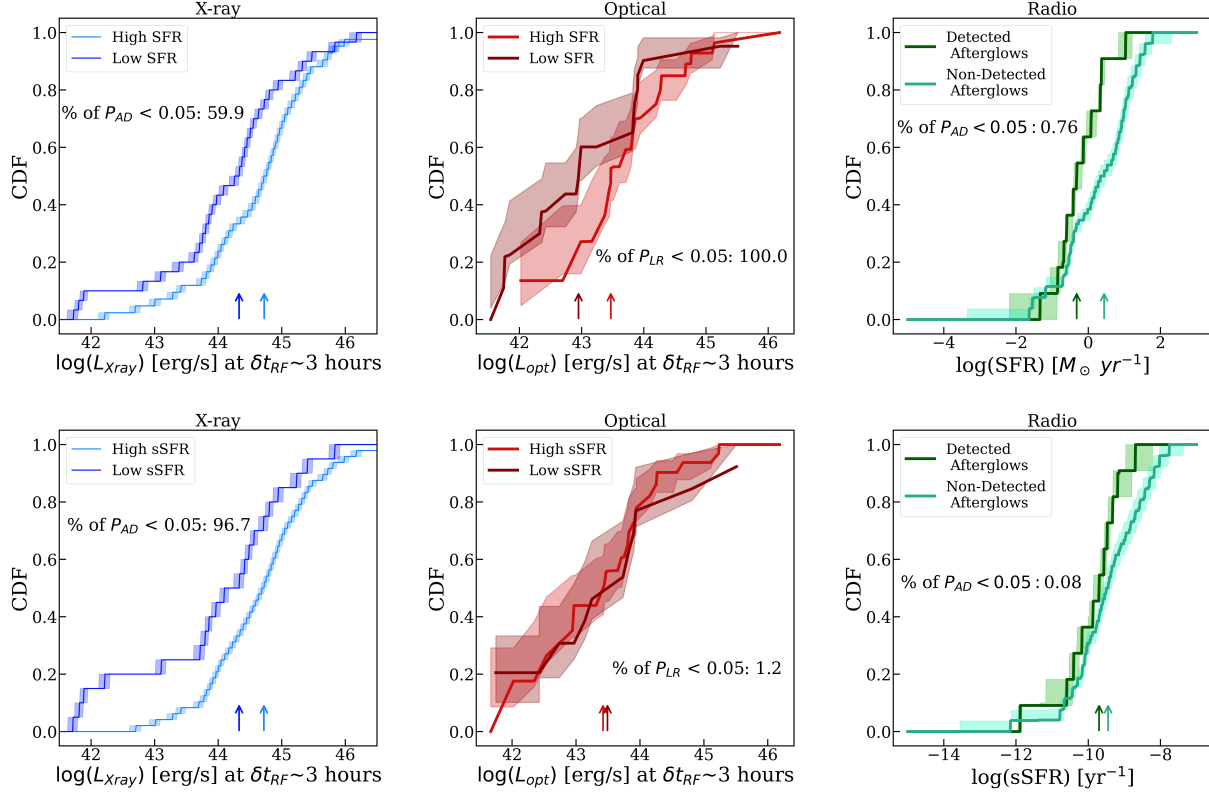


**Figure 4.** The same as Figure 3, except for SFR and sSFR. For the X-ray and optical afterglow CDFs, the lighter lines represent the short GRBs with  $SFR > 1 M_{\odot} \text{ yr}^{-1}$  or  $\log(\text{sSFR}) > -10 \text{ yr}^{-1}$ , and the darker lines show the short GRBs with  $SFR < 1 M_{\odot} \text{ yr}^{-1}$  or  $\log(\text{sSFR}) < -10 \text{ yr}^{-1}$ . We find that short GRB X-ray and optical afterglows are more luminous in host galaxies with higher SFR, and X-ray afterglows are additionally brighter in hosts with higher sSFR. In the radio band, it appears that non-detections occur more often in more actively star-forming galaxies but do not pass the threshold for statistical significance.

For optical afterglows, Figure 4 shows that hosts with higher SFR overall have brighter optical afterglows compared to those with lower SFR. However, the higher and lower sSFR distributions are not as distinct as both distributions have larger overlap. Using a logrank test to compare the SFR distributions with upper limits, we find that  $100\% p_{LR} < 0.05$ , rejecting the null hypothesis that the two distributions are drawn from the same underlying one. However, we find that the difference *is not* statistically significant for the sSFR distributions, with only  $1.2\% p_{LR} < 0.05$ . Thus, this likely indicates that optical afterglows only have a weak dependence on the amount of active star formation in the host. When we perform the same analysis at  $\delta t_c = 10 \text{ hr}$ , we do find statistical significance for SFR, but do not for sSFR.

As in the previous section, we investigate if radio afterglows are correlated with host galaxy SFR or sSFR by computing the relevant distributions for the populations of GRBs with radio afterglows detections (11 events) versus only upper limits (27 events). To accurately probe the uncertainty on SFR and sSFR for

the populations of short GRBs with afterglow detections and with only upper limits, we randomly sample 5000 values for each GRB from the SFR and sSFR posteriors provided on the BRIGHT repository (Nugent et al. 2022). We then build 5000 CDFs from these samples. We find that the median SFR and sSFR for bursts with radio detections is smaller ( $0.5^{+1.8}_{-0.4} M_{\odot} \text{ yr}^{-1}$  and  $\log(\text{sSFR}) = -9.7^{+0.2}_{-0.1} \text{ yr}^{-1}$ ), than those of non-detections ( $2.1^{+15.4}_{-1.9} M_{\odot} \text{ yr}^{-1}$  and  $\log(\text{sSFR}) = -9.5^{+1.1}_{-0.1} \text{ yr}^{-1}$ ). We show the 5000 CDFs of SFRs and sSFRs for the population of GRBs with radio afterglow detections and upper limits in Figure 4. Performing an AD test for the SFR distributions, we find that only 1% of  $p_{AD} < 0.05$  failing to reject the null hypothesis. Similarly for sSFR, we find that 0.1% of  $p_{AD} < 0.05$ , and that the difference *is not* statistically significant. Thus, we do not find a clear correlation between star-formation in a host galaxy and detectability of radio afterglows.

Overall, we find that short GRB X-ray and optical afterglows are more luminous in host galaxies that have more active star formation, with X-ray afterglows having

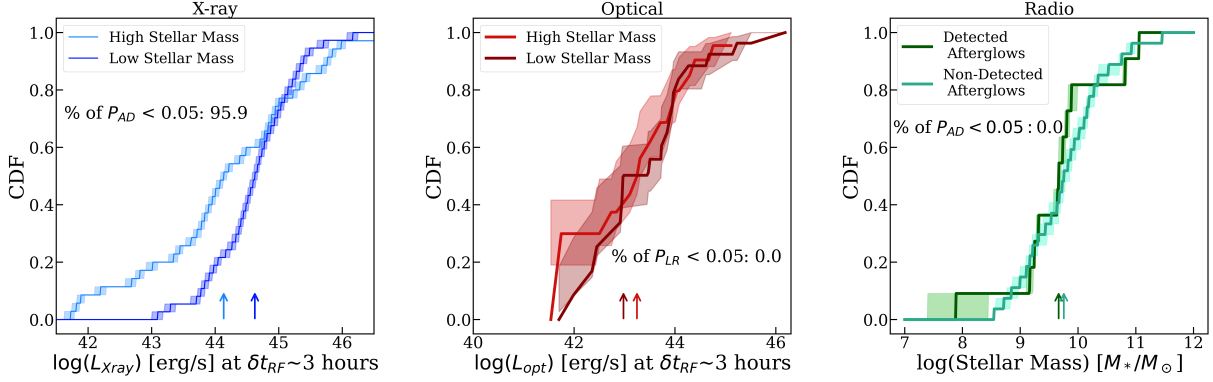


**Figure 5.** The same as Figure 3, except for stellar mass. For the X-ray and optical afterglow CDFs, the lighter lines represent the short GRBs with  $\log(M_*/M_\odot) > 9.7$  and the darker lines show the short GRBs in host galaxies with  $\log(M_*/M_\odot) < 9.7$ . We find that short GRBs in host galaxies with less stellar mass have brighter X-ray afterglows, although we do not find any correlation between  $\log(M_*/M_\odot)$  and optical afterglow luminosity or radio afterglow detection.

a stronger dependence on the amount of star formation in their hosts. However, we do not find a trend in the radio band as the result does not pass the threshold for statistical significance. Our results overall support the picture that the higher expected ISM densities in more star-forming hosts give way to brighter short GRB afterglows.

#### 4.4. Stellar Mass

We next compare afterglows to host galaxy stellar mass ( $M_*$ ). Since quiescent galaxies are typically older and more massive than star-forming galaxies (Blanton & Moustakas 2009; Leja et al. 2022; Tacchella et al. 2022), we can form a reasonable assumption that short GRBs in more massive hosts have less luminous afterglows. This is already hinted at by the fact that we find afterglows in the X-ray (optical) bands are less luminous in low SFR and sSFR (low SFR) galaxies (Section 4.3). To investigate this, we divide our sample at the median host stellar mass ( $\approx 10^{9.7} M_\odot$ ; Nugent et al. 2022) into low-mass and high-mass hosts. After building the CDFs in the X-ray band, as expected, the events in hosts with lower stellar masses overall have brighter X-ray afterglows than the events in higher stellar mass hosts (Figure 5). This is statistically supported by our AD test, in which 96% of the  $p_{AD} < 0.05$ , rejecting the null hypothesis that the two luminosity distributions are drawn from the same underlying one. The same conclusion is drawn when we perform the test at  $\delta t_c = 10$  hr. This is commensurate with our findings that X-ray afterglows are brighter in hosts with higher SFR and sSFR.

In the optical band, we find that the events that occur in hosts with lower stellar masses also appear to have brighter optical afterglows, although there is overlap at high luminosities (Figure 5). This visual difference is not supported statistically, as we find that 0% of our

$p_{LR} < 0.05$ . In contrast to our conclusion with X-ray afterglows, we find that there is no statistical evidence that short GRBs in lower mass hosts have distinct optical afterglow luminosities than those in higher mass hosts despite the visual differences, which stays true when we perform the same tests on detections alone, and for  $\delta t_c = 10$  hr.

Finally, we investigate any trends for radio afterglows by computing stellar mass distributions for the populations that have radio afterglows detections (11) versus upper limits (27), following the same methods of capturing the uncertainty on the stellar mass distributions as described for SFR and sSFR (Section 4.3). For the population of short GRBs with radio afterglow detections, we find a median and 68% confidence interval of  $\log(M_*/M_\odot) = 9.7^{+1.1}_{-0.2}$ , and a median and 68% confidence interval of  $\log(M_*/M_\odot) = 9.8^{+0.5}_{-0.1} M_*/M_\odot$  for the population with upper limits. We show the 5000 CDFs of the stellar masses for the population of GRBs with radio afterglow detections and upper limits in Figure 5. When comparing the distributions with an AD test, we find that 0% of the  $p_{AD} < 0.05$ , failing to reject the null hypothesis that the two distributions are drawn from the same underlying distribution. Thus, we find no support that the detectability of radio afterglows are correlated with stellar mass.

#### 4.5. Stellar Population Age

Finally, we compare afterglows to host galaxy mass-weighted stellar population age ( $t_m$ ). As previously mentioned, quiescent galaxies are typically older and more massive than star-forming galaxies. Thus, given our previous findings, we expect to find that short GRBs in younger hosts will have more luminous afterglows than those in older hosts. To investigate this, we divide our sample at the median  $t_m$  ( $\approx 0.8$  Gyr; Nugent

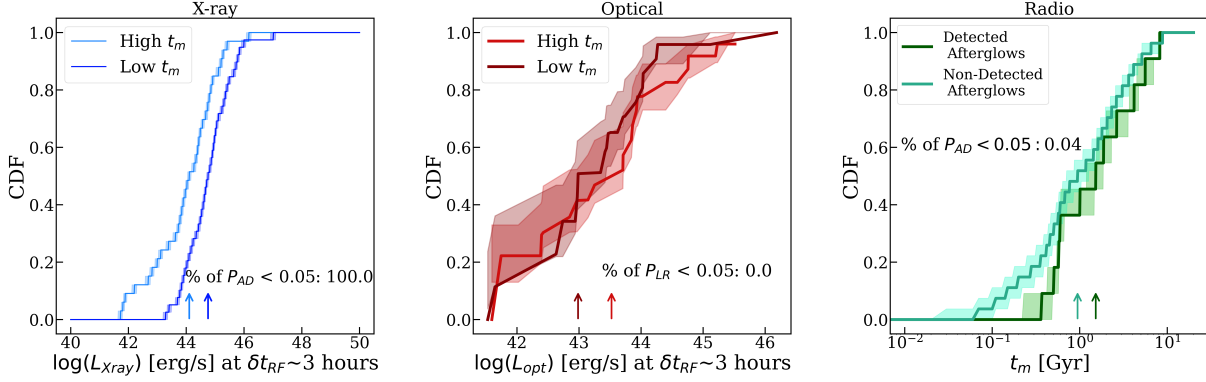


**Figure 6.** The same as Figure 3, except for host galaxy stellar population age ( $t_m$ ). For the X-ray and optical afterglow CDFs, the lighter lines represent the short GRBs with  $t_m > 0.8$  Gyr and the darker lines show the short GRBs with  $t_m < 0.8$  Gyr. We find that short GRBs in host galaxies with lower  $t_m$  have brighter X-ray afterglows, although we do not find any correlation between  $t_m$  and optical afterglow luminosity or radio afterglow detection.

et al. 2022) into low  $t_m$  (younger) and high  $t_m$  (older) hosts. We find that short GRBs in younger hosts have brighter X-ray afterglows than the events in older hosts (Figure 6). This is statistically supported by our AD test, in which 100% of the  $p_{AD} < 0.05$ , rejecting the null hypothesis that the two luminosity distributions are drawn from the same underlying one. The same result is found at  $\delta t_c = 10$  hr.

We do not find the same trend when inspecting the luminosity distributions at high and low  $t_m$  in the optical band (Figure 6), as there is significant overlap between the distributions. When comparing the distributions with the logrank test, we furthermore determine that 0% of our  $p_{LR} < 0.05$  (the same holds true when performing the test for detections only, and also at  $\delta t_c = 10$  hr for both detections and upper limits). Thus, in contrast to our conclusion with X-ray afterglows, we find that there is no statistical evidence that short GRBs in younger hosts have distinct optical afterglow luminosities than those in older hosts.

Lastly, we compare the distributions of  $t_m$  between the population of GRBs with detected radio afterglows and upper limits. We show the CDFs of  $t_m$  for these two populations in Figure 6 and build uncertainties on the CDFs in the same manner as described for SFR and stellar mass (Sections 4.3–4.4). While visually it appears that the population of short GRBs with detected radio afterglows trend toward larger  $t_m$  (median and 68% confidence interval  $1.51^{+3.48}_{-0.97}$  Gyr) than those with only upper limits (median and 68% confidence interval  $0.95^{+2.79}_{-0.69}$ ), we find that 0% of the 5000 AD tests performed between the populations result in  $p_{AD} < 0.05$ . Thus, we do not find any statistical evidence that detectability of radio afterglows is correlated with  $t_m$ .

## 5. DISCUSSION

### 5.1. Implications for Local Environments

In this paper, we test whether short GRB afterglow brightness correlates with properties of the kiloparsec-scale environments. The baseline expectation is that brighter afterglows should originate in environments with higher ISM densities - we would typically expect this for GRBs that occur at smaller galactocentric offsets and in host galaxies with higher amounts of active star formation, younger stellar population ages and lower stellar masses. Overall, we find agreement with these expectations, although we do not always find the results to be statistically significant across all wavelengths. To visualize this, in Figure 7, we plot the fraction of  $p_{AD}$  or  $p_{LR}$  values that meet the threshold to refute the null hypothesis ( $p < 0.05$ ), where a fraction of  $> 50\%$  indicates statistically distinct luminosity distributions in that property. We show these values across all tested properties in the X-ray, optical and radio bands.

From Figure 7, it is clear that no wavelength has statistically distinct afterglow luminosity distributions across *all* properties. We find that X-ray and radio afterglows are brighter or more likely to be detected for GRBs at smaller offsets from their hosts. We also visualize the same trend for optical afterglows, but we cannot recover a statistically significant distinction. We further find that X-ray afterglows are brighter when they occur in hosts with higher amount of star formation (SFR and sSFR), lower stellar mass, and lower stellar population age – again aligning with all expectations. However, while we also visualize these differences for optical afterglows, the only statistically significant trend we can recover is that they are brighter in hosts with higher SFR; no other tested stellar population property yields a statistical distinction. Finally, we find no other statistically significant trends in the radio band beyond off-

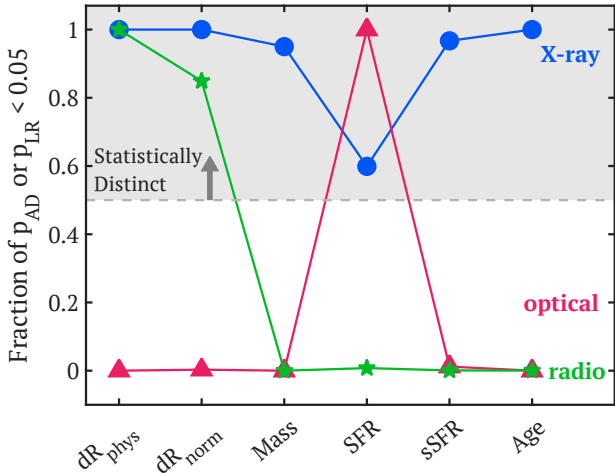


**Figure 7.** The fraction of  $p_{AD}$  or  $p_{LR}$  values that are  $< 0.05$  when assessing whether distributions of “high” and “low” (e.g., high-offset and low-offset) environmental properties are drawn from the same underlying distribution. We show the fraction for the X-ray (blue circles), optical (red triangles) and radio (green stars) bands across our tested properties. Fractions above 0.5 are considered to be support for statistically distinct distributions. Overall, X-ray afterglows align most with expectations, while we only recover statistically significant trends for the radio and optical afterglows in offset and SFR/sSFR, respectively.

sets. Taken together, our results demonstrate that the X-ray afterglow luminosity is the most predictable indicator of underlying host properties. Given the visual differences in optical afterglow luminosity distributions, it is possible that increasing the sample size of optical afterglows and/or obtaining deeper afterglow detections and upper limits will lead to a statistical distinction in the future.

We next connect these results to expectations from the local environments. The synchrotron afterglow model provides expectations for how the afterglow brightness maps to local environment (i.e., circumburst density  $n_0$ ) and intrinsic burst properties (energetics, microphysics). Indeed, in the slow-cooling regime, the radio, optical and X-ray bands all share a dependence on circumburst density ( $F_\nu \propto n_0^{1/2}$  for  $\nu_a < \nu < \nu_m$  and  $\nu_m < \nu < \nu_c$ , where  $\nu_a$ ,  $\nu_m$ , and  $\nu_c$  are the self-absorption, maximum, and cooling break frequencies, respectively; Granot & Sari 2002). Thus, all else being equal, afterglows in higher-density environments should be brighter<sup>7</sup> (as shown in the radio band; i.e., Schroeder et al. 2025). The fact

that we only recover statistically significant trends with global host properties in the X-ray band could mean that we do not have enough detections to claim statistical significance in the optical or radio bands, that the local and global environmental properties are not strongly linked, or that other factors such as energetics and microphysics play a strong role in afterglow brightness.

## 5.2. Merger-Driven Long GRBs and GW Events

We next turn to the population of long GRBs that likely originate from mergers (“merger-driven LGRBs”; c.f., Jin et al. 2015; Yang et al. 2015; Rastinejad et al. 2022a; Troja et al. 2022; Yang et al. 2022; Gillanders et al. 2023; Levan et al. 2024; Yang et al. 2024), and compare their afterglow luminosities to those of short GRBs. For this comparison, we consider GRBs 060614, 211211A and 230307A as part of the merger-driven LGRB class. We use our analysis to investigate whether their afterglows are systematically brighter than the rest of our sample, as would be expected if they were LGRBs that originated from collapsars (e.g., Gehrels et al. 2008). For each environmental property, we compare each GRB’s luminosity to the relevant luminosity distribution (i.e., high or low in a given property, as described in Section 4). Using the values from Table B2, we find that all three merger-driven LGRBs fall into the low-SFR and low-mass categories. In terms of offset, GRB 060614 falls into the low-offset bin, while GRBs 211211A and 230307A are considered high-offset bursts. Finally, for stellar population age, GRB 060614 has a young age, while the latter two are in the older age category.

In Figure 8, we plot the population medians and uncertainties (68% confidence) in X-ray and optical afterglow luminosities, split by “high” and “low”-values for each tested property. For comparison, we plot the locations of the three merger-driven LGRBs as well as GW170817 (if it was on-axis, see below). Overall, we find that their X-ray afterglow luminosities are unremarkable compared to the relevant short GRB luminosity distribution (in which  $\approx 30 - 60\%$  of short GRBs are fainter). For optical afterglows, while GRBs 060614 and 211211A are on the fainter end compared to the population (for which only  $\approx 0 - 33\%$  of afterglows are fainter), we find that GRB 230307A is very bright in the optical band: at the  $\approx 92 - 96\%$  in brightness, although it is not the brightest. However, this trend is not echoed in the X-rays, as its X-ray afterglow is relatively faint, at the  $\approx 11 - 37\%$  level when compared to the relevant short GRBs. Overall, we do not find clear distinctions between the known merger-driven LGRBs and the traditional short GRB population, lending support that these three events do in fact arise from mergers.

<sup>7</sup> The exception is if the X-ray band is above the cooling frequency ( $\nu_X > \nu_c$ ) in which case the afterglow brightness is independent of density (Granot & Sari 2002).

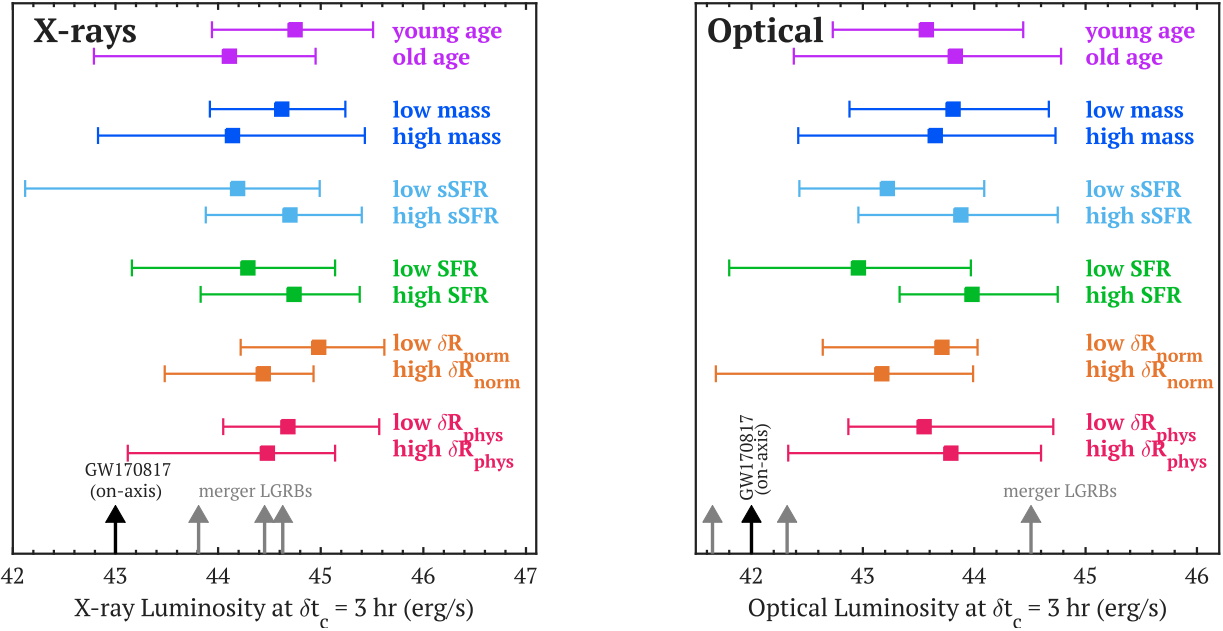


**Figure 8.** Median X-ray (left) and optical (right) afterglow luminosities in which the length of each bar represents the 68% confidence interval for each population, representing the values in Table 1. Each color represents a different property, split into high- and low-value sub-populations. Overall, we find that short GRB X-ray afterglows are brighter for hosts with younger ages, lower masses, higher SFRs and sSFRs, and for bursts at lower galactocentric offsets. We find that optical afterglows are only brighter in hosts with higher SFR.

Another highly relevant application of this research is understanding its utility in strategies for follow-up of gravitational-wave (GW) events. Short GRBs are intrinsically related to the local population of GW sources from the association of short GRB 170817A to neutron star (NS) merger GW170817 (Abbott et al. 2017). Despite the prevalence of follow-up campaigns for subsequent GW-detected binary NS and NS-black hole mergers, there have been no other credible associations of these events to GRBs, afterglow emission, or KNe (Andreoni et al. 2019; Coughlin et al. 2019; Dobie et al. 2019; Goldstein et al. 2019; Gomez et al. 2019; Hosseinzadeh et al. 2019; Lundquist et al. 2019; Ackley et al. 2020; Andreoni et al. 2020; Antier et al. 2020a,b; Garcia et al. 2020; Gompertz et al. 2020; Kasliwal et al. 2020; Morgan et al. 2020; Pozanenko et al. 2020; Thakur et al. 2020; Vieira et al. 2020; Watson et al. 2020; Alexander et al. 2021; Anand et al. 2021; Becerra et al. 2021; Bhakta et al. 2021; Chang et al. 2021; de Wet et al. 2021b; Dichiara et al. 2021; Kilpatrick et al. 2021; Oates et al. 2021; Ohgami et al. 2021; Paterson et al. 2021; Tucker et al. 2022; de Jaeger et al. 2022; Dobie et al. 2022; Rastinejad et al. 2022b; Ahumada et al. 2024). However, the lack of detectable electromagnetic counterparts may not be surprising if most other GW-NS mergers are similar to GW170817. The host of GW170817 (NGC4993

has been characterized as massive ( $\approx 10^{10.6} M_{\odot}$ ), quiescent ( $SFR \approx 0.02 M_{\odot} \text{ yr}^{-1}$ ), and old ( $\approx 10.4 \text{ Gyr}$ ; Blanchard et al. 2017; Levan et al. 2017; Palmese et al. 2017; Pan et al. 2017; Kilpatrick et al. 2022). Nugent et al. (2022) places NGC4993 in the top 84% of stellar masses for short GRB hosts, and determines that it has the lowest SFR (and sSFR) and highest stellar population age compared to all other short GRB hosts (c.f., Figure 8). Although GW170817 has a small galactocentric offset ( $\approx 2 \text{ kpc}$ ), which would generally correlate with a brighter afterglow from our analysis, the rest of its environmental properties indicate that GW170817/GRB170817A should have had a faint afterglow compared to most short GRBs.

We next more fully test how the afterglow of GRB 170817A compares to expectations from its host properties given our analysis. First, for direct comparison to our short GRB population, we approximate the X-ray and optical afterglow luminosities of GRB 170817A had it been *on-axis*, since its true observing angle was  $\sim 20^\circ$  (Margutti et al. 2017; Lazzati et al. 2018; Lyman et al. 2018; Resmi et al. 2018; Troja et al. 2018b; Hotokezaka et al. 2019; Lamb et al. 2019a; Ghirlanda et al. 2019; Salafia et al. 2019; Margutti & Chornock 2021). Using the Wu & MacFadyen (2019) on-axis model, we find that X-ray and optical afterglow lu-

minosities of  $L_X \approx 10^{43}$  erg s $^{-1}$  and  $L_{\text{opt}} \approx 10^{42}$  erg s $^{-1}$  at  $\delta t_c = 3$  hr. These luminosities are perfectly in alignment with our expectations of a GRB in a quiescent, old and massive environment. The X-ray and optical afterglows are on the faint end when compared to the relevant luminosity distributions (low SFR and sSFR, high stellar mass), with only  $\approx 13 - 29\%$  of afterglows that are fainter (Figure 8). Meanwhile, we note that no events in the low stellar mass category ( $< 10^{9.7} M_\odot$ ) have such a low X-ray afterglow luminosity, and only 2-5% of GRBs with  $\text{SFR} > 1 M_\odot \text{ yr}^{-1}$  and  $\text{sSFR} > 10^{-10} \text{ yr}^{-1}$  have similarly low X-ray afterglow luminosities. We find similar results in the optical band: no GRBs in high SFR hosts have such a low optical afterglow luminosity and only 6-16% of GRBs with low stellar mass and high sSFR have lower optical afterglow luminosities.

Thus, if most other local Universe GW-mergers occur in similar environments to GW170817, we expect that their afterglow luminosities will be faint and difficult to detect, especially if the event is more offset from its host (as GW170817 has a low galactocentric offset compared to the short GRB population); this will only be exacerbated because most GW mergers will be off-axis. However, given the diversity of short GRB environments, with the majority in less massive, star-forming galaxies than the host of GW170817, we expect their afterglows to be commensurately brighter. Furthermore, as next generation GW detectors will expand merger populations out to higher redshifts, where the fraction of star-forming galaxies increases, the likelihood of detecting (intrinsically) brighter afterglows may increase. Finally, we note that upcoming observing missions, such as the Vera Rubin Observatory (LSST Science Collaboration et al. 2009) and the Roman Observatory (Akeson et al. 2019), promise to detect transient emission out to  $\approx 26$  mag, which will greatly help in detecting faint optical afterglow emission that may be a result of the GRB environment.

## 6. CONCLUSION

In this paper, we leverage a large sample of short GRB X-ray, optical and radio afterglow data, combined with properties of the GRB environment from uniform host galaxy modeling, to investigate correlations between afterglows and hosts. Our tested environmental properties include physical and host normalized galactocentric offsets, host SFR, sSFR, stellar mass, and stellar population age. Our full sample contains 150 short GRBs observed between 2005-2023, and thus comprises the most extensive exploration of GRB afterglows and their environments to-date. To fairly compare all X-ray and optical afterglow luminosities to environmen-

tal properties, we formulate a new method to determine a luminosity at a common rest-frame time ( $L_c$ ) of  $\delta t_c = 3$  hours, taking advantage of the full lightcurves in these bands. We then compare the X-ray and optical  $L_c$  distributions, divided at (or near) the median value of environmental property of interest. As radio afterglow data is sparse for our short GRB population, we focus our analysis in this band to environmental properties between GRBs with detected and non-detected afterglows. We come to the following conclusions:

- At small galactocentric offsets (physical and host-normalized;  $< 7$  kpc,  $< 1.66 r_e$ ), we find that short GRB X-ray afterglows are more luminous, while radio afterglows are more detectable. Optical afterglows for short GRBs at small offsets also appear to be brighter, but the distinction relative to high-offset short GRBs is not statistically significant.
- Compared to the expectation that afterglows should be brighter in younger galaxies with higher SFRs or sSFRs and lower stellar masses, we find statistical evidence that X-ray afterglows fully agree with these expectations. In contrast, for optical afterglows, the only statistically significant correlation we find is that they are brighter in galaxies with high SFR. Taken together, our results demonstrate that the X-ray afterglow luminosity is the most predictable indicator of underlying host properties.
- From a comparison of the three merger-driven LGRBs (GRBs 060614, 211211A and 230307A) to the traditional short GRB population, we find that their afterglow luminosities are unremarkable compared to the short GRB population. This lends support to the idea that these LGRBs derive from mergers, as opposed to collapsars, which we would expect have brighter afterglows.
- We estimate the afterglow luminosities of GW170817/GRB 170817A had it been *on-axis*, finding that its inferred X-ray and optical afterglows are on the faint end compared to the short GRB population (with  $\approx 13 - 29\%$  of events fainter in the respective host categories). This aligns well with the expectation that less luminous afterglows arise in quiescent, old and massive environments. Given the correlations we have found, if the host environments of future GW-detected mergers are similar, this may translate to lower afterglow luminosities.

We finally note that it is peculiar that there are less correlations between environmental properties and optical afterglows than there are for environmental properties and X-ray afterglows. Indeed, if afterglow luminosity is correlated with ISM density, than we would expect, for example, to find stronger correlations between optical afterglow luminosity and galactocentric offsets. We postulate that this lack of correlations in the optical band is due to instrument sensitivity, as optical afterglows fade so rapidly that they can quickly go below the detection limit of most optical observatories currently used for follow-up. With the onset of operations of the Vera C. Rubin Observatory, and the upcoming planned *Nancy Grace Roman* telescope, the promise of discovering the faintest optical and infrared afterglows may be realized. Rubin and *Roman* will also enable detection of the faintest galaxies, thus aiding in characterizing the low-mass and high-redshift GRB hosts. Finally, twenty years of NASA's *Swift* Observatory operations have provided an unparalleled opportunity to explore the relationship between short GRBs and their host galaxies. We look forward to the next era of short GRB science, and their crucial connection to multi-messenger counterparts.

#### ACKNOWLEDGEMENTS

We are forever grateful to the Neil Gehrels *Swift* Observatory, its continued mission to observe GRBs and their afterglows after two decades in-flight, and its ability to inspire new generations of time-domain astronomers.

We acknowledge Jillian Rastinejad for informative discussions. C.C. acknowledges support for this project from the Weinberg Summer Research Grant, the Summer Undergraduate Research Grant from Northwestern University's Office of Undergraduate Research, and the NASA Illinois Space Grant Consortium. The material contained in this document is based upon work sup-

ported in part by a National Aeronautics and Space Administration (NASA) grant or cooperative agreement. Any opinions, findings, conclusions, or recommendations expressed in this material are those of the author and do not necessarily reflect the views of NASA. This work was in part supported through a NASA grant awarded to the Illinois/NASA Space Grant Consortium.

The Fong Group at Northwestern acknowledges support by the National Science Foundation under grant Nos. AST-1909358, AST-2206494, AST-2308182, and CAREER grant No. AST-2047919. The Villar Astro Time Lab acknowledges support through the David and Lucile Packard Foundation, the Research Corporation for Scientific Advancement (through a Cottrell Fellowship), the National Science Foundation under AST-2433718, AST-2407922 and AST-2406110, as well as an Aramont Fellowship for Emerging Science Research. W.F. gratefully acknowledges support by the David and Lucile Packard Foundation, the Alfred P. Sloan Foundation, and the Research Corporation for Science Advancement through Cottrell Scholar Award #28284.

The Villar Astro Time Lab acknowledges support through the David and Lucile Packard Foundation, the Research Corporation for Scientific Advancement (through a Cottrell Fellowship), the National Science Foundation under AST-2433718, AST-2407922 and AST-2406110, as well as an Aramont Fellowship for Emerging Science Research. This work is supported by the National Science Foundation under Cooperative Agreement PHY-2019786 (the NSF AI Institute for Artificial Intelligence and Fundamental Interactions).

We acknowledge the use of public data from the *Swift* data archive.

*Facilities:* *Swift* (XRT)

*Software:* Astropy (Astropy Collaboration et al. 2022), Scipy, lifelines (Davidson-Pilon 2019)

#### REFERENCES

- Abbott, B. P., Abbott, R., Abbott, T. D., et al. 2017, ApJL, 848, L13, doi: [10.3847/2041-8213/aa920c](https://doi.org/10.3847/2041-8213/aa920c)
- Ackley, K., Amati, L., Barbieri, C., et al. 2020, A&A, 643, A113, doi: [10.1051/0004-6361/202037669](https://doi.org/10.1051/0004-6361/202037669)
- Agüí Fernández, J. F., Thöne, C. C., Kann, D. A., et al. 2023, MNRAS, 520, 613, doi: [10.1093/mnras/stad099](https://doi.org/10.1093/mnras/stad099)
- Ahumada, T., Singer, L. P., Anand, S., et al. 2021, Nature Astronomy, 5, 917, doi: [10.1038/s41550-021-01428-7](https://doi.org/10.1038/s41550-021-01428-7)
- Ahumada, T., Anand, S., Coughlin, M. W., et al. 2024, PASP, 136, 114201, doi: [10.1088/1538-3873/ad8265](https://doi.org/10.1088/1538-3873/ad8265)
- Akeson, R., Armus, L., Bachelet, E., et al. 2019, arXiv e-prints, arXiv:1902.05569, doi: [10.48550/arXiv.1902.05569](https://doi.org/10.48550/arXiv.1902.05569)
- Alexander, K. D., Schroeder, G., Paterson, K., et al. 2021, ApJ, 923, 66, doi: [10.3847/1538-4357/ac281a](https://doi.org/10.3847/1538-4357/ac281a)
- Anand, N., Shahid, M., & Resmi, L. 2018, MNRAS, 481, 4332, doi: [10.1093/mnras/sty2530](https://doi.org/10.1093/mnras/sty2530)
- Anand, S., Coughlin, M. W., Kasliwal, M. M., et al. 2021, Nature Astronomy, 5, 46, doi: [10.1038/s41550-020-1183-3](https://doi.org/10.1038/s41550-020-1183-3)
- Anderson, G. E., Bell, M. E., Stevens, J., et al. 2018, GRB Coordinates Network, 23467, 1

- . 2020, GRB Coordinates Network, 27573, 1
- Anderson, G. E., Bell, M. E., Hancock, P. J., et al. 2022, GRB Coordinates Network, 32529, 1
- Anderson, G. E., Stevens, J., Bell, M. E., et al. 2023, GRB Coordinates Network, 33433, 1
- Andreoni, I., Goldstein, D. A., Anand, S., et al. 2019, ApJL, 881, L16, doi: [10.3847/2041-8213/ab3399](https://doi.org/10.3847/2041-8213/ab3399)
- Andreoni, I., Goldstein, D. A., Kasliwal, M. M., et al. 2020, ApJ, 890, 131, doi: [10.3847/1538-4357/ab6a1b](https://doi.org/10.3847/1538-4357/ab6a1b)
- Andrews, J. J., & Mandel, I. 2019, ApJL, 880, L8, doi: [10.3847/2041-8213/ab2ed1](https://doi.org/10.3847/2041-8213/ab2ed1)
- Antier, S., Agayeva, S., Aivazyan, V., et al. 2020a, MNRAS, 492, 3904, doi: [10.1093/mnras/stz3142](https://doi.org/10.1093/mnras/stz3142)
- Antier, S., Agayeva, S., Almualla, M., et al. 2020b, MNRAS, 497, 5518, doi: [10.1093/mnras/staa1846](https://doi.org/10.1093/mnras/staa1846)
- Astropy Collaboration, Robitaille, T. P., Tollerud, E. J., et al. 2013, A&A, 558, A33, doi: [10.1051/0004-6361/201322068](https://doi.org/10.1051/0004-6361/201322068)
- Astropy Collaboration, Price-Whelan, A. M., Sipőcz, B. M., et al. 2018, AJ, 156, 123, doi: [10.3847/1538-3881/aabc4f](https://doi.org/10.3847/1538-3881/aabc4f)
- Astropy Collaboration, Price-Whelan, A. M., Lim, P. L., et al. 2022, ApJ, 935, 167, doi: [10.3847/1538-4357/ac7c74](https://doi.org/10.3847/1538-4357/ac7c74)
- Becerra, R. L., Dichiara, S., Watson, A. M., et al. 2021, MNRAS, 507, 1401, doi: [10.1093/mnras/stab2086](https://doi.org/10.1093/mnras/stab2086)
- Belkin, S., Klunko, E., Pozanenko, A., Pankov, N., & GRB IKI FuN. 2023, GRB Coordinates Network, 33383, 1
- Belles, A., D’Ai, A., & Swift/UVOT Team. 2021, GRB Coordinates Network, 31222, 1
- Bennett, C. L., Larson, D., Weiland, J. L., & Hinshaw, G. 2014, ApJ, 794, 135, doi: [10.1088/0004-637X/794/2/135](https://doi.org/10.1088/0004-637X/794/2/135)
- Berger, E. 2007, ApJ, 670, 1254, doi: [10.1086/522195](https://doi.org/10.1086/522195)
- . 2014, ARA&A, 52, 43, doi: [10.1146/annurev-astro-081913-035926](https://doi.org/10.1146/annurev-astro-081913-035926)
- Berger, E., Cenko, S. B., Fox, D. B., & Cucchiara, A. 2009, ApJ, 704, 877, doi: [10.1088/0004-637X/704/1/877](https://doi.org/10.1088/0004-637X/704/1/877)
- Berger, E., & Fong, W. 2009a, GRB Coordinates Network, 10182, 1
- Berger, E., Fong, W., & Chornock, R. 2013a, ApJL, 774, L23, doi: [10.1088/2041-8205/774/2/L23](https://doi.org/10.1088/2041-8205/774/2/L23)
- Berger, E., & Fong, W. F. 2009b, GRB Coordinates Network, 9373, 1
- . 2009c, GRB Coordinates Network, 9555, 1
- . 2009d, GRB Coordinates Network, 9683, 1
- Berger, E., Price, P. A., Cenko, S. B., et al. 2005, Nature, 438, 988, doi: [10.1038/nature04238](https://doi.org/10.1038/nature04238)
- Berger, E., Fox, D. B., Price, P. A., et al. 2007, ApJ, 664, 1000, doi: [10.1086/518762](https://doi.org/10.1086/518762)
- Berger, E., Zauderer, B. A., Levan, A., et al. 2013b, ApJ, 765, 121, doi: [10.1088/0004-637X/765/2/121](https://doi.org/10.1088/0004-637X/765/2/121)
- Bhakta, D., Mooley, K. P., Corsi, A., et al. 2021, ApJ, 911, 77, doi: [10.3847/1538-4357/abeaa8](https://doi.org/10.3847/1538-4357/abeaa8)
- Bigiel, F., & Blitz, L. 2012, ApJ, 756, 183, doi: [10.1088/0004-637X/756/2/183](https://doi.org/10.1088/0004-637X/756/2/183)
- Blanchard, P. K., Berger, E., & Fong, W.-f. 2016, ApJ, 817, 144, doi: [10.3847/0004-637X/817/2/144](https://doi.org/10.3847/0004-637X/817/2/144)
- Blanchard, P. K., Berger, E., Fong, W., et al. 2017, ApJL, 848, L22, doi: [10.3847/2041-8213/aa9055](https://doi.org/10.3847/2041-8213/aa9055)
- Blanton, M. R., & Moustakas, J. 2009, ARA&A, 47, 159, doi: [10.1146/annurev-astro-082708-101734](https://doi.org/10.1146/annurev-astro-082708-101734)
- Blustin, A. J., Mangano, V., Voges, W., Marshall, F., & Gehrels, N. 2005a, GRB Coordinates Network, 4331, 1
- Blustin, A. J., Retter, A., Page, M. J., et al. 2005b, GRB Coordinates Network, 3791, 1
- Bolmer, J., Steinle, H., & Schady, P. 2017, GRB Coordinates Network, 21050, 1
- Breeveld, A. A., Dichiara, S., & Swift/UVOT Team. 2023, GRB Coordinates Network, 33392, 1
- Breeveld, A. A., Groppi, J. D., & Swift/UVOT Team. 2021, GRB Coordinates Network, 29712, 1
- Breeveld, A. A., & Krimm, H. A. 2015, GRB Coordinates Network, 18092, 1
- Breeveld, A. A., Page, K. L., & Swift/UVOT Team. 2020, GRB Coordinates Network, 29129, 1
- Breeveld, A. A., & Siegel, M. H. 2016, GRB Coordinates Network, 19839, 1
- Brout, D., & Scolnic, D. 2021, ApJ, 909, 26, doi: [10.3847/1538-4357/abd69b](https://doi.org/10.3847/1538-4357/abd69b)
- Brown, P. J., & Pagani, C. 2008, GRB Coordinates Network, 8208, 1
- Brown, P. J., & Racusin, J. L. 2006, GRB Coordinates Network, 5385, 1
- Burns, E., Goldstein, A., Lesage, S., Dalessi, S., & Fermi-GBM Team. 2023, GRB Coordinates Network, 33414, 1
- Butler, N., Watson, A. M., Kutyrev, A., et al. 2015, GRB Coordinates Network, 17762, 1
- . 2016, GRB Coordinates Network, 19131, 1
- . 2018, GRB Coordinates Network, 22582, 1
- . 2019, GRB Coordinates Network, 26121, 1
- Cameron, P. B., & Frail, D. A. 2005a, GRB Coordinates Network, 3815, 1
- . 2005b, GRB Coordinates Network, 3933, 1
- Cano, Z., Heintz, K. E., Malesani, D., & Tronsgaard, R. 2017, GRB Coordinates Network, 20549, 1
- Capalbi, M., Kennea, J. A., Tohuvavohu, A., et al. 2023, GRB Coordinates Network, 33365, 1
- Cardelli, J. A., Clayton, G. C., & Mathis, J. S. 1989, ApJ, 345, 245, doi: [10.1086/167900](https://doi.org/10.1086/167900)

- Casasola, V., Cassarà, L. P., Bianchi, S., et al. 2017, A&A, 605, A18, doi: [10.1051/0004-6361/201731020](https://doi.org/10.1051/0004-6361/201731020)
- Casentini, C., Tavani, M., Pittori, C., et al. 2023, GRB Coordinates Network, 33412, 1
- Castro-Tirado, A. J., Bond, I., Kilmartin, P., et al. 2005, GRB Coordinates Network, 3018, 1
- Cenko, S. B., Fox, D. B., & Price, P. A. 2006, GRB Coordinates Network, 5912, 1
- Chandra, P., Cenko, S. B., Frail, D. A., & Harrison, F. 2008, GRB Coordinates Network, 8451, 1
- Chandra, P., & Frail, D. A. 2006, GRB Coordinates Network, 5910, 1
- . 2007a, GRB Coordinates Network, 6367, 1
- . 2007b, GRB Coordinates Network, 6685, 1
- . 2007c, GRB Coordinates Network, 6667, 1
- . 2007d, GRB Coordinates Network, 6742, 1
- . 2007e, GRB Coordinates Network, 6831, 1
- . 2008a, GRB Coordinates Network, 7934, 1
- . 2008b, GRB Coordinates Network, 8419, 1
- . 2009, GRB Coordinates Network, 9160, 1
- Chandra, P., & Nayana, A. J. 2017, GRB Coordinates Network, 21441, 1
- Chang, S.-W., Onken, C. A., Wolf, C., et al. 2021, PASA, 38, e024, doi: [10.1017/pasa.2021.17](https://doi.org/10.1017/pasa.2021.17)
- Chastain, S. I., van der Horst, A. J., Anderson, G. E., et al. 2024, MNRAS, 532, 2820, doi: [10.1093/mnras/stae1568](https://doi.org/10.1093/mnras/stae1568)
- Chen, T. W., Klose, S., Guelbenzu, A. N., et al. 2016, GRB Coordinates Network, 19975, 1
- Chester, M. M., & D'Elia, V. 2015, GRB Coordinates Network, 17323, 1
- Childress, M., Aldering, G., Antilogus, P., et al. 2013, ApJ, 770, 108, doi: [10.1088/0004-637X/770/2/108](https://doi.org/10.1088/0004-637X/770/2/108)
- Choi, C., Kim, Y., Park, W., Shin, S., & Im, M. 2018, GRB Coordinates Network, 22668, 1
- Chornock, R., & Fong, W. 2015, GRB Coordinates Network, 17358, 1
- Chrimes, A. A., Gompertz, B. P., Kann, D. A., et al. 2022, Monthly Notices of the Royal Astronomical Society, 515, 2591–2611, doi: [10.1093/mnras/stac1796](https://doi.org/10.1093/mnras/stac1796)
- Church, R. P., Levan, A. J., Davies, M. B., & Tanvir, N. 2011, MNRAS, 413, 2004, doi: [10.1111/j.1365-2966.2011.18277.x](https://doi.org/10.1111/j.1365-2966.2011.18277.x)
- Coughlin, M. W., Ahumada, T., Anand, S., et al. 2019, ApJL, 885, L19, doi: [10.3847/2041-8213/ab4ad8](https://doi.org/10.3847/2041-8213/ab4ad8)
- Coulter, D. A., Kilpatrick, C. D., Jones, D. O., et al. 2024, arXiv e-prints, arXiv:2404.15441, doi: [10.48550/arXiv.2404.15441](https://doi.org/10.48550/arXiv.2404.15441)
- Cucchiara, A., Morris, D., & Guidorzi, C. 2017, GRB Coordinates Network, 21382, 1
- Cucchiara, A., & Ukwatta, T. N. 2008, GRB Coordinates Network, 7207, 1
- Dai, C.-Y., Guo, C.-L., Zhang, H.-M., Liu, R.-Y., & Wang, X.-Y. 2024, ApJL, 962, L37, doi: [10.3847/2041-8213/ad2680](https://doi.org/10.3847/2041-8213/ad2680)
- D'Andrea, C. B., Gupta, R. R., Sako, M., et al. 2011, ApJ, 743, 172, doi: [10.1088/0004-637X/743/2/172](https://doi.org/10.1088/0004-637X/743/2/172)
- d'Antonio, D., Bell, M. E., Anderson, G. E., et al. 2020, GRB Coordinates Network, 27245, 1
- D'Avanzo, P., D'Elia, V., Malesani, D., et al. 2017, GRB Coordinates Network, 21055, 1
- D'Avanzo, P., Piranomonte, S., Di Fabrizio, L., Stoev, H., & CIBO Collaboration. 2022, GRB Coordinates Network, 31904, 1
- D'Avanzo, P., Malesani, D., Covino, S., et al. 2009, A&A, 498, 711, doi: [10.1051/0004-6361/200811294](https://doi.org/10.1051/0004-6361/200811294)
- D'Avanzo, P., Salvaterra, R., Sbarufatti, B., et al. 2012, MNRAS, 425, 506, doi: [10.1111/j.1365-2966.2012.21489.x](https://doi.org/10.1111/j.1365-2966.2012.21489.x)
- D'Avanzo, P., Rossi, A., Brivio, R., et al. 2023, GRB Coordinates Network, 33374, 1
- Davidson-Pilon, C. 2019, Journal of Open Source Software, 4, 1317, doi: [10.21105/joss.01317](https://doi.org/10.21105/joss.01317)
- de Jaeger, T., Shappee, B. J., Kochanek, C. S., et al. 2022, MNRAS, 509, 3427, doi: [10.1093/mnras/stab3141](https://doi.org/10.1093/mnras/stab3141)
- de Pasquale, M. 2008, GRB Coordinates Network, 7932, 1
- de Pasquale, M., & D'Ai, A. 2016, GRB Coordinates Network, 19576, 1
- de Pasquale, M., & Kocevski, D. 2015, GRB Coordinates Network, 18753, 1
- de Pasquale, M., Kuin, N. P., & Krimm, H. A. 2016, GRB Coordinates Network, 19465, 1
- de Pasquale, M., & Stratta, G. 2008, GRB Coordinates Network, 8406, 1
- de Ugarte Postigo, A., Kann, D. A., Malesani, D. B., et al. 2021a, GRB Coordinates Network, 29717, 1
- de Ugarte Postigo, A., Kann, D. A., Thoene, C., et al. 2021b, GRB Coordinates Network, 31218, 1
- de Wet, S., Vreeswijk, P. M., Levan, A. J., et al. 2021a, GRB Coordinates Network, 31063, 1
- de Wet, S., Groot, P. J., Bloemen, S., et al. 2021b, A&A, 649, A72, doi: [10.1051/0004-6361/202040231](https://doi.org/10.1051/0004-6361/202040231)
- Dezalay, J. P., Barat, C., Talon, R., et al. 1992, in American Institute of Physics Conference Series, Vol. 265, American Institute of Physics Conference Series, ed. W. S. Paciesas & G. J. Fishman (AIP), 304
- Dichiara, S., Cenko, S. B., Troja, E., et al. 2020a, GRB Coordinates Network, 28572, 1
- Dichiara, S., O'Connor, B., & Troja, E. 2020b, GRB Coordinates Network, 27822, 1

- Dichiara, S., & Troja, E. 2019, GRB Coordinates Network, 26147, 1
- Dichiara, S., Troja, E., Cenko, S. B., et al. 2020c, GRB Coordinates Network, 29128, 1
- Dichiara, S., Becerra, R. L., Chase, E. A., et al. 2021, ApJL, 923, L32, doi: [10.3847/2041-8213/ac4259](https://doi.org/10.3847/2041-8213/ac4259)
- Dimple, Panchal, A., Gangopadhyay, A., et al. 2020, GRB Coordinates Network, 29148, 1
- Dobie, D., Stewart, A., Murphy, T., et al. 2019, ApJL, 887, L13, doi: [10.3847/2041-8213/ab59db](https://doi.org/10.3847/2041-8213/ab59db)
- Dobie, D., Stewart, A., Hotokezaka, K., et al. 2022, MNRAS, 510, 3794, doi: [10.1093/mnras/stab3628](https://doi.org/10.1093/mnras/stab3628)
- Elenin, L., Mazaeva, E., Volnova, A., Molotov, I., & Pozanenko, A. 2016, GRB Coordinates Network, 19127, 1
- Emery, S. W. K., & Beardmore, A. P. 2016, GRB Coordinates Network, 19134, 1
- Emery, S. W. K., & Lien, A. Y. 2018, GRB Coordinates Network, 22587, 1
- Evans, P. A., & Swift-XRT Team. 2023, GRB Coordinates Network, 33379, 1
- Evans, P. A., Beardmore, A. P., Page, K. L., et al. 2007, A&A, 469, 379, doi: [10.1051/0004-6361:20077530](https://doi.org/10.1051/0004-6361:20077530)
- . 2009, MNRAS, 397, 1177, doi: [10.1111/j.1365-2966.2009.14913.x](https://doi.org/10.1111/j.1365-2966.2009.14913.x)
- Fong, W. 2016, GRB Coordinates Network, 19147, 1
- Fong, W., & Berger, E. 2013, ApJ, 776, 18, doi: [10.1088/0004-637X/776/1/18](https://doi.org/10.1088/0004-637X/776/1/18)
- Fong, W., Berger, E., Margutti, R., & Zauderer, B. A. 2015, ApJ, 815, 102, doi: [10.1088/0004-637X/815/2/102](https://doi.org/10.1088/0004-637X/815/2/102)
- Fong, W., Laskar, T., Alexander, K. D., & Berger, E. 2017, GRB Coordinates Network, 21395, 1
- Fong, W., Tanvir, N. R., & Levan, A. J. 2018a, GRB Coordinates Network, 23439, 1
- Fong, W., Tanvir, N. R., Levan, A. J., & Chornock, R. 2018b, GRB Coordinates Network, 22659, 1
- Fong, W., Berger, E., Margutti, R., et al. 2012, ApJ, 756, 189, doi: [10.1088/0004-637X/756/2/189](https://doi.org/10.1088/0004-637X/756/2/189)
- Fong, W., Berger, E., Metzger, B. D., et al. 2014, ApJ, 780, 118, doi: [10.1088/0004-637X/780/2/118](https://doi.org/10.1088/0004-637X/780/2/118)
- Fong, W., Margutti, R., Chornock, R., et al. 2016, ApJ, 833, 151, doi: [10.3847/1538-4357/833/2/151](https://doi.org/10.3847/1538-4357/833/2/151)
- Fong, W., Laskar, T., Rastinejad, J., et al. 2021, ApJ, 906, 127, doi: [10.3847/1538-4357/abc74a](https://doi.org/10.3847/1538-4357/abc74a)
- Fong, W.-f., Nugent, A. E., Dong, Y., et al. 2022, ApJ, 940, 56, doi: [10.3847/1538-4357/ac91d0](https://doi.org/10.3847/1538-4357/ac91d0)
- Fox, D. B., & Cenko, S. B. 2005, GRB Coordinates Network, 3787, 1
- Fox, D. B., Frail, D. A., Price, P. A., et al. 2005, Nature, 437, 845, doi: [10.1038/nature04189](https://doi.org/10.1038/nature04189)
- Frail, D. A. 2005, GRB Coordinates Network, 4276, 1
- Frail, D. A., & Cameron, P. B. 2005, GRB Coordinates Network, 4199, 1
- Frail, D. A., & Chandra, P. 2008, GRB Coordinates Network, 7684, 1
- . 2009, GRB Coordinates Network, 9354, 1
- Frail, D. A., & Soderberg, A. M. 2005, GRB Coordinates Network, 3007, 1
- Frail, D. A., Kulkarni, S. R., Sari, R., et al. 2001, ApJL, 562, L55, doi: [10.1086/338119](https://doi.org/10.1086/338119)
- Fruchter, A. S., Levan, A. J., Strolger, L., et al. 2006, Nature, 441, 463, doi: [10.1038/nature04787](https://doi.org/10.1038/nature04787)
- Fu, S. Y., Zhu, Z. P., Liu, X., et al. 2021, GRB Coordinates Network, 29700, 1
- Fynbo, J. U., Jensen, B. L., Gorosabel, J., et al. 2001, A&A, 369, 373, doi: [10.1051/0004-6361:20010112](https://doi.org/10.1051/0004-6361:20010112)
- Garcia, A., Morgan, R., Herner, K., et al. 2020, ApJ, 903, 75, doi: [10.3847/1538-4357/abb823](https://doi.org/10.3847/1538-4357/abb823)
- Gaspari, N., Levan, A. J., Chrimes, A. A., & Nelemans, G. 2024, MNRAS, 527, 1101, doi: [10.1093/mnras/stad3259](https://doi.org/10.1093/mnras/stad3259)
- Gehrels, N., Chincarini, G., Giommi, P., et al. 2004, ApJ, 611, 1005, doi: [10.1086/422091](https://doi.org/10.1086/422091)
- Gehrels, N., Barthelmy, S. D., Burrows, D. N., et al. 2008, ApJ, 689, 1161, doi: [10.1086/592766](https://doi.org/10.1086/592766)
- Ghirlanda, G., Salafia, O. S., Paragi, Z., et al. 2019, Science, 363, 968, doi: [10.1126/science.aau8815](https://doi.org/10.1126/science.aau8815)
- Gillanders, J. H., Troja, E., Fryer, C. L., et al. 2023, arXiv e-prints, arXiv:2308.00633, doi: [10.48550/arXiv.2308.00633](https://doi.org/10.48550/arXiv.2308.00633)
- Goldstein, A., Veres, P., Burns, E., et al. 2017, ApJL, 848, L14, doi: [10.3847/2041-8213/aa8f41](https://doi.org/10.3847/2041-8213/aa8f41)
- Goldstein, D. A., Andreoni, I., Nugent, P. E., et al. 2019, ApJL, 881, L7, doi: [10.3847/2041-8213/ab3046](https://doi.org/10.3847/2041-8213/ab3046)
- Gomez, S., Hosseinzadeh, G., Cowperthwaite, P. S., et al. 2019, ApJL, 884, L55, doi: [10.3847/2041-8213/ab4ad5](https://doi.org/10.3847/2041-8213/ab4ad5)
- Gompertz, B. P., Nicholl, M., Tanvir, N., et al. 2022, GRB Coordinates Network, 32966, 1
- Gompertz, B. P., Levan, A. J., Tanvir, N. R., et al. 2018, ApJ, 860, 62, doi: [10.3847/1538-4357/aac206](https://doi.org/10.3847/1538-4357/aac206)
- Gompertz, B. P., Cutter, R., Steeghs, D., et al. 2020, MNRAS, 497, 726, doi: [10.1093/mnras/staa1845](https://doi.org/10.1093/mnras/staa1845)
- Graham, J., Bolmer, J., Wiseman, P., & Greiner, J. 2016, GRB Coordinates Network, 19144, 1
- Graham, J. F., Fruchter, A. S., Levan, A. J., et al. 2009, ApJ, 698, 1620, doi: [10.1088/0004-637X/698/2/1620](https://doi.org/10.1088/0004-637X/698/2/1620)
- Granot, J., & Sari, R. 2002, ApJ, 568, 820, doi: [10.1086/338966](https://doi.org/10.1086/338966)
- Gropp, J. D., D’Elia, V., & Swift/UVOT Team. 2019, GRB Coordinates Network, 26128, 1
- Grossan, B., Komesh, T., Maksut, Z., et al. 2021, GRB Coordinates Network, 31016, 1

- Guidorzi, C., Kobayashi, S., Mundell, C. G., Gomboc, A., & Steele, I. A. 2018a, GRB Coordinates Network, 22792, 1
- Guidorzi, C., Martone, R., Kobayashi, S., et al. 2018b, GRB Coordinates Network, 22648, 1
- Gupta, R. R., D'Andrea, C. B., Sako, M., et al. 2011, ApJ, 740, 92, doi: [10.1088/0004-637X/740/2/92](https://doi.org/10.1088/0004-637X/740/2/92)
- Hancock, P., Murphy, T., Gaensler, B., et al. 2012a, GRB Coordinates Network, 13338, 1
- . 2012b, GRB Coordinates Network, 13611, 1
- Hao, J.-M., & Yuan, Y.-F. 2013, A&A, 558, A22, doi: [10.1051/0004-6361/201321471](https://doi.org/10.1051/0004-6361/201321471)
- Harita, S., Fujiwara, T., Yoshii, T., et al. 2015, GRB Coordinates Network, 17763, 1
- Heintz, K. E., Tanvir, N. R., Perley, D. A., & Rasmussen, R. T. 2017, GRB Coordinates Network, 21374, 1
- Higgins, A., Wiersema, K., & Malesani, D. B. 2018, GRB Coordinates Network, 23090, 1
- Hinshaw, G., Larson, D., Komatsu, E., et al. 2013, ApJS, 208, 19, doi: [10.1088/0067-0049/208/2/19](https://doi.org/10.1088/0067-0049/208/2/19)
- Holland, S. T., & Marshall, F. E. 2006, GRB Coordinates Network, 5898, 1
- Horiuchi, T., Hanayama, H., Honma, M., et al. 2018, GRB Coordinates Network, 22670, 1
- Hosokawa, R., Imai, Y., Murata, K. L., et al. 2021, GRB Coordinates Network, 31031, 1
- Hosseinzadeh, G., Cowperthwaite, P. S., Gomez, S., et al. 2019, ApJL, 880, L4, doi: [10.3847/2041-8213/ab271c](https://doi.org/10.3847/2041-8213/ab271c)
- Hotokezaka, K., Nakar, E., Gottlieb, O., et al. 2019, Nature Astronomy, 3, 940, doi: [10.1038/s41550-019-0820-1](https://doi.org/10.1038/s41550-019-0820-1)
- Hoversten, E. A., & Godet, O. 2008, GRB Coordinates Network, 8737, 1
- Hu, Y. D., Casanova, V., Fernandez-Garcia, E., et al. 2023, GRB Coordinates Network, 33387, 1
- Hu, Y. D., Fernandez-Garcia, E., Castro-Tirado, A. J., et al. 2020, GRB Coordinates Network, 27784, 1
- Hu, Y. D., Casanova, V., Sun, T. R., et al. 2021, GRB Coordinates Network, 30976, 1
- Immler, S., & Holland, S. T. 2008, GRB Coordinates Network, 8277, 1
- Ito, N., Hosokawa, R., Murata, K. L., et al. 2020, GRB Coordinates Network, 28571, 1
- . 2021, GRB Coordinates Network, 31217, 1
- Jeong, M., & Im, M. 2024, ApJ, 974, 114, doi: [10.3847/1538-4357/ad6b2a](https://doi.org/10.3847/1538-4357/ad6b2a)
- Jeong, S., Im, M., Choi, C., & Lim, G. 2016a, GRB Coordinates Network, 19140, 1
- Jeong, S., & Lee, C.-H. 2010, Journal of the Korean Physical Society, 56, 1619, doi: [10.3938/jkps.56.1619](https://doi.org/10.3938/jkps.56.1619)
- Jeong, S., Park, I. H., Hu, Y., Scarpa, R., & Castro-Tirado, A. J. 2016b, GRB Coordinates Network, 19847, 1
- Jiang, S. Q., Zhu, Z. P., Fu, S. Y., et al. 2021, GRB Coordinates Network, 31213, 1
- Jin, Z.-P., Covino, S., Liao, N.-H., et al. 2020, Nature Astronomy, 4, 77, doi: [10.1038/s41550-019-0892-y](https://doi.org/10.1038/s41550-019-0892-y)
- Jin, Z.-P., Li, X., Cano, Z., et al. 2015, ApJL, 811, L22, doi: [10.1088/2041-8205/811/2/L22](https://doi.org/10.1088/2041-8205/811/2/L22)
- Jin, Z.-P., Hotokezaka, K., Li, X., et al. 2016, Nature Communications, 7, 12898, doi: [10.1038/ncomms12898](https://doi.org/10.1038/ncomms12898)
- Johnson, S., Reichart, D., Haislip, J., et al. 2007, GRB Coordinates Network, 6218, 1
- Kann, D. A., de Ugarte Postigo, A., Thoene, C. C., et al. 2021, GRB Coordinates Network, 30992, 1
- Kann, D. A., Tanga, M., & Greiner, J. 2015, GRB Coordinates Network, 17757, 1
- Kann, D. A., Klose, S., Zhang, B., et al. 2010, ApJ, 720, 1513, doi: [10.1088/0004-637X/720/2/1513](https://doi.org/10.1088/0004-637X/720/2/1513)
- . 2011, ApJ, 734, 96, doi: [10.1088/0004-637X/734/2/96](https://doi.org/10.1088/0004-637X/734/2/96)
- Kasliwal, M. M., Korobkin, O., Lau, R. M., Wollaeger, R., & Fryer, C. L. 2017, ApJL, 843, L34, doi: [10.3847/2041-8213/aa799d](https://doi.org/10.3847/2041-8213/aa799d)
- Kasliwal, M. M., Anand, S., Ahumada, T., et al. 2020, ApJ, 905, 145, doi: [10.3847/1538-4357/abc335](https://doi.org/10.3847/1538-4357/abc335)
- Kelly, P. L., Hicken, M., Burke, D. L., Mandel, K. S., & Kirshner, R. P. 2010, ApJ, 715, 743, doi: [10.1088/0004-637X/715/2/743](https://doi.org/10.1088/0004-637X/715/2/743)
- Kilpatrick, C. D., Coulter, D. A., Arcavi, I., et al. 2021, ApJ, 923, 258, doi: [10.3847/1538-4357/ac23c6](https://doi.org/10.3847/1538-4357/ac23c6)
- Kilpatrick, C. D., Fong, W.-f., Blanchard, P. K., et al. 2022, ApJ, 926, 49, doi: [10.3847/1538-4357/ac3e59](https://doi.org/10.3847/1538-4357/ac3e59)
- Kim, S., Im, M., Cooke, J., et al. 2021, GRB Coordinates Network, 30856, 1
- Kinugasa, K., Honda, S., Hashimoto, O., Takahashi, H., & Taguchi, H. 2009, GRB Coordinates Network, 9292, 1
- Klose, S., Nicuesa Guelbenzu, A., Kruehler, T., Malesani, D., & Greiner, J. 2016, GRB Coordinates Network, 19142, 1
- Knust, F., Klose, S., & Greiner, J. 2015, GRB Coordinates Network, 18219, 1
- Komesh, T., Maksut, Z., Grossan, B., et al. 2023, GRB Coordinates Network, 33436, 1
- Kouveliotou, C., Meegan, C. A., Fishman, G. J., et al. 1993, ApJL, 413, L101, doi: [10.1086/186969](https://doi.org/10.1086/186969)
- Krühler, T., Greiner, J., Schady, P., et al. 2011, A&A, 534, A108, doi: [10.1051/0004-6361/201117428](https://doi.org/10.1051/0004-6361/201117428)
- Kuin, N. P. M., & Beardmore, A. P. 2017, GRB Coordinates Network, 21049, 1
- Kuin, N. P. M., & D'Avanzo, P. 2018, GRB Coordinates Network, 23080, 1
- Kuin, N. P. M., Dichiara, S., & Swift/UVOT Team. 2021, GRB Coordinates Network, 30975, 1

- . 2022a, GRB Coordinates Network, 32435, 1
- Kuin, N. P. M., Evans, P. A., & Swift/UVOT Team. 2020a, GRB Coordinates Network, 27783, 1
- Kuin, N. P. M., & Hoversten, E. A. 2009, GRB Coordinates Network, 9342, 1
- Kuin, N. P. M., & Page, K. L. 2016, GRB Coordinates Network, 19970, 1
- Kuin, N. P. M., Tohuvavohu, A., & Swift/UVOT Team. 2020b, GRB Coordinates Network, 27539, 1
- Kuin, P., Eyles-Ferris, R., & Swift/UVOT Team. 2022b, GRB Coordinates Network, 32958, 1
- Kuin, P., & Gibson, S. L. 2016, GRB Coordinates Network, 19963, 1
- Kumar, H., Swain, V., Norbu, R., et al. 2022, GRB Coordinates Network, 31892, 1
- Kumar, H., Bhalerao, V., Gupta, R., et al. 2021, GRB Coordinates Network, 31227, 1
- Kuroda, D., Yanagisawa, K., & Kawai, N. 2008, GRB Coordinates Network, 7676, 1
- Kuroda, D., Yanagisawa, K., Shimizu, Y., et al. 2015a, GRB Coordinates Network, 17742, 1
- . 2015b, GRB Coordinates Network, 18761, 1
- . 2016a, GRB Coordinates Network, 19128, 1
- . 2016b, GRB Coordinates Network, 19480, 1
- Kuroda, D., Hanayama, H., Miyaji, T., et al. 2016c, GRB Coordinates Network, 19571, 1
- Lamb, G. P., Lyman, J. D., Levan, A. J., et al. 2019a, ApJL, 870, L15, doi: [10.3847/2041-8213/aaf96b](https://doi.org/10.3847/2041-8213/aaf96b)
- Lamb, G. P., Tanvir, N. R., Levan, A. J., et al. 2019b, ApJ, 883, 48, doi: [10.3847/1538-4357/ab38bb](https://doi.org/10.3847/1538-4357/ab38bb)
- Lampeitl, H., Smith, M., Nichol, R. C., et al. 2010, ApJ, 722, 566, doi: [10.1088/0004-637X/722/1/566](https://doi.org/10.1088/0004-637X/722/1/566)
- Laporte, S. 2017, GRB Coordinates Network, 21399, 1
- Laporte, S. J., & Cannizzo, J. K. 2017, GRB Coordinates Network, 21386, 1
- Laporte, S. J., & Cenko, S. B. 2017, GRB Coordinates Network, 21388, 1
- Laskar, T., Fong, W., Alexander, K. D., et al. 2019, GRB Coordinates Network, 26120, 1
- Laskar, T., Escorial, A. R., Schroeder, G., et al. 2022, ApJL, 935, L11, doi: [10.3847/2041-8213/ac8421](https://doi.org/10.3847/2041-8213/ac8421)
- Lazzati, D., Perna, R., Morsony, B. J., et al. 2018, PhRvL, 120, 241103, doi: [10.1103/PhysRevLett.120.241103](https://doi.org/10.1103/PhysRevLett.120.241103)
- Leibler, C. N., & Berger, E. 2010, ApJ, 725, 1202, doi: [10.1088/0004-637X/725/1/1202](https://doi.org/10.1088/0004-637X/725/1/1202)
- Leja, J., Speagle, J. S., Ting, Y.-S., et al. 2022, ApJ, 936, 165, doi: [10.3847/1538-4357/ac887d](https://doi.org/10.3847/1538-4357/ac887d)
- Levan, A. J., Rastinejad, J., Gompertz, B., et al. 2021, GRB Coordinates Network, 31235, 1
- Levan, A. J., Tanvir, N. R., Fruchter, A. S., et al. 2006, ApJL, 648, L9, doi: [10.1086/507625](https://doi.org/10.1086/507625)
- Levan, A. J., Tanvir, N. R., Jakobsson, P., et al. 2008, MNRAS, 384, 541, doi: [10.1111/j.1365-2966.2007.11953.x](https://doi.org/10.1111/j.1365-2966.2007.11953.x)
- Levan, A. J., Lyman, J. D., Tanvir, N. R., et al. 2017, ApJL, 848, L28, doi: [10.3847/2041-8213/aa905f](https://doi.org/10.3847/2041-8213/aa905f)
- Levan, A. J., Gompertz, B. P., Salafia, O. S., et al. 2024, Nature, 626, 737, doi: [10.1038/s41586-023-06759-1](https://doi.org/10.1038/s41586-023-06759-1)
- Lien, A., Sakamoto, T., Barthelmy, S. D., et al. 2016, ApJ, 829, 7, doi: [10.3847/0004-637X/829/1/7](https://doi.org/10.3847/0004-637X/829/1/7)
- Lipunov, V., Gorbovskoy, E., Kornilov, V., et al. 2020a, GRB Coordinates Network, 27542, 1
- . 2020b, GRB Coordinates Network, 29122, 1
- . 2020c, GRB Coordinates Network, 27789, 1
- Lipunov, V., Kornilov, V., Gorbovskoy, E., et al. 2021, GRB Coordinates Network, 31216, 1
- Littlejohns, O., Butler, N., Watson, A. M., et al. 2015, GRB Coordinates Network, 17736, 1
- LSST Science Collaboration, Abell, P. A., Allison, J., et al. 2009, arXiv e-prints, arXiv:0912.0201, doi: [10.48550/arXiv.0912.0201](https://doi.org/10.48550/arXiv.0912.0201)
- Lu, T. H., Jiang, S. Q., Fu, S. Y., et al. 2023, GRB Coordinates Network, 33381, 1
- Lundquist, M. J., Paterson, K., Fong, W., et al. 2019, ApJL, 881, L26, doi: [10.3847/2041-8213/ab32f2](https://doi.org/10.3847/2041-8213/ab32f2)
- Lyman, J. D., Levan, A. J., Tanvir, N. R., et al. 2017, MNRAS, 467, 1795, doi: [10.1093/mnras/stx220](https://doi.org/10.1093/mnras/stx220)
- Lyman, J. D., Lamb, G. P., Levan, A. J., et al. 2018, Nature Astronomy, 2, 751, doi: [10.1038/s41550-018-0511-3](https://doi.org/10.1038/s41550-018-0511-3)
- MacFadyen, A. I., & Woosley, S. E. 1999, ApJ, 524, 262, doi: [10.1086/307790](https://doi.org/10.1086/307790)
- Malesani, D., Heintz, K. E., Stone, M., & Stone, J. 2018, GRB Coordinates Network, 22660, 1
- Malesani, D., Uthas, H., Thoene, C. C., et al. 2007a, GRB Coordinates Network, 6254, 1
- Malesani, D., Xu, D., & Kuutma, T. 2016, GRB Coordinates Network, 19300, 1
- Malesani, D., Covino, S., D'Avanzo, P., et al. 2007b, A&A, 473, 77, doi: [10.1051/0004-6361:20077868](https://doi.org/10.1051/0004-6361:20077868)
- Malesani, D. B., de Ugarte Postigo, A., Zhu, Z., et al. 2021a, GRB Coordinates Network, 29703, 1
- Malesani, D. B., & Knudstrup, E. 2020, GRB Coordinates Network, 29117, 1
- Malesani, D. B., Fynbo, J. P. U., de Ugarte Postigo, A., et al. 2021b, GRB Coordinates Network, 31221, 1
- Margutti, R., & Chornock, R. 2021, ARA&A, 59, 155, doi: [10.1146/annurev-astro-112420-030742](https://doi.org/10.1146/annurev-astro-112420-030742)
- Margutti, R., Berger, E., Fong, W., et al. 2012, ApJ, 756, 63, doi: [10.1088/0004-637X/756/1/63](https://doi.org/10.1088/0004-637X/756/1/63)

- Margutti, R., Zaninoni, E., Bernardini, M. G., et al. 2013, MNRAS, 428, 729, doi: [10.1093/mnras/sts066](https://doi.org/10.1093/mnras/sts066)
- Margutti, R., Berger, E., Fong, W., et al. 2017, ApJL, 848, L20, doi: [10.3847/2041-8213/aa9057](https://doi.org/10.3847/2041-8213/aa9057)
- Marshall, F. E., & Beardmore, A. 2018, GRB Coordinates Network, 23062, 1
- Marshall, F. E., & Beardmore, A. P. 2015, GRB Coordinates Network, 17751, 1
- Marshall, F. E., & Cannizzo, J. K. 2017, GRB Coordinates Network, 20554, 1
- Marshall, F. E., & Gibson, S. L. 2016, GRB Coordinates Network, 19275, 1
- Marshall, F. E., Groppi, J. D., & Swift/UVOT Team. 2020, GRB Coordinates Network, 28565, 1
- Marshall, F. E., & Pagani, C. 2015, GRB Coordinates Network, 17739, 1
- Mazaeva, E., Kusakin, A., Pozanenko, A., et al. 2018, GRB Coordinates Network, 22809, 1
- Mazaeva, E., Reva, I., Volnova, A., & Pozanenko, A. 2015a, GRB Coordinates Network, 18097, 1
- Mazaeva, E., Volnova, A., Kusakin, A., & Pozanenko, A. 2015b, GRB Coordinates Network, 17750, 1
- Melandri, A., Burgdorf, M., Smith, R. J., et al. 2008, GRB Coordinates Network, 8402, 1
- Meldorf, C., Palmese, A., Brout, D., et al. 2023, MNRAS, 518, 1985, doi: [10.1093/mnras/stac3056](https://doi.org/10.1093/mnras/stac3056)
- Meszaros, P., & Rees, M. J. 1993, ApJ, 405, 278, doi: [10.1086/172360](https://doi.org/10.1086/172360)
- Moin, A., Frail, D. A., Tingay, S., & Macquart, J. P. 2009a, GRB Coordinates Network, 10021, 1
- Moin, A., Tingay, S., Phillips, C., et al. 2009b, GRB Coordinates Network, 8952, 1
- . 2009c, GRB Coordinates Network, 8953, 1
- Mooley, K. P., Staley, T. D., Fender, R. P., et al. 2017a, GRB Coordinates Network, 20958, 1
- . 2017b, GRB Coordinates Network, 21058, 1
- . 2017c, GRB Coordinates Network, 21212, 1
- . 2017d, GRB Coordinates Network, 21466, 1
- . 2017e, GRB Coordinates Network, 21465, 1
- Morgan, R., Soares-Santos, M., Annis, J., et al. 2020, ApJ, 901, 83, doi: [10.3847/1538-4357/abafaa](https://doi.org/10.3847/1538-4357/abafaa)
- Mori, Y. A., Shimokawabe, T., Kudou, Y., Nakajima, H., & Kawai, N. 2008, GRB Coordinates Network, 7929, 1
- Muraki, Y., Ono, Y., Fujiwara, T., et al. 2016, GRB Coordinates Network, 19285, 1
- Murata, K. L., Miyakawa, K., & Nagayama, T. 2016, GRB Coordinates Network, 19999, 1
- Murata, K. L., Niwano, M., Imai, Y., et al. 2022, GRB Coordinates Network, 31889, 1
- Nakajima, H., Shimokawabe, T., Mori, Y. A., Kudou, Y., & Kawai, N. 2008, GRB Coordinates Network, 8202, 1
- Nakar, E. 2007, PhR, 442, 166, doi: [10.1016/j.physrep.2007.02.005](https://doi.org/10.1016/j.physrep.2007.02.005)
- Nakar, E., Gal-Yam, A., & Fox, D. B. 2006, ApJ, 650, 281, doi: [10.1086/505855](https://doi.org/10.1086/505855)
- Neill, J. D., Sullivan, M., Howell, D. A., et al. 2009, ApJ, 707, 1449, doi: [10.1088/0004-637X/707/2/1449](https://doi.org/10.1088/0004-637X/707/2/1449)
- Nicuesa Guelbenzu, A., Klose, S., & Rau, A. 2021, GRB Coordinates Network, 31069, 1
- Niino, Y., Aoki, K., Hashimoto, T., et al. 2017, PASJ, 69, 27, doi: [10.1093/pasj/psw133](https://doi.org/10.1093/pasj/psw133)
- Noonan, K., Orange, N., Gokuldass, P., et al. 2023, GRB Coordinates Network, 33426, 1
- Norris, J. P., Cline, T. L., Desai, U. D., & Teegarden, B. J. 1984, Nature, 308, 434, doi: [10.1038/308434a0](https://doi.org/10.1038/308434a0)
- Nousek, J. A., Kouveliotou, C., Grupe, D., et al. 2006, ApJ, 642, 389, doi: [10.1086/500724](https://doi.org/10.1086/500724)
- Nugent, A. E., Fong, W.-f., Castrejon, C., et al. 2024, ApJ, 962, 5, doi: [10.3847/1538-4357/ad17c0](https://doi.org/10.3847/1538-4357/ad17c0)
- Nugent, A. E., Ji, A. P., Fong, W.-f., Shah, H., & van de Voort, F. 2025, ApJ, 982, 144, doi: [10.3847/1538-4357/adbb6a](https://doi.org/10.3847/1538-4357/adbb6a)
- Nugent, A. E., Fong, W., Dong, Y., et al. 2020, ApJ, 904, 52, doi: [10.3847/1538-4357/abc24a](https://doi.org/10.3847/1538-4357/abc24a)
- Nugent, A. E., Fong, W.-F., Dong, Y., et al. 2022, ApJ, 940, 57, doi: [10.3847/1538-4357/ac91d1](https://doi.org/10.3847/1538-4357/ac91d1)
- Nysewander, M., Fruchter, A., & Graham, J. 2007, GRB Coordinates Network, 6604, 1
- Nysewander, M., Fruchter, A. S., & Pe'er, A. 2009, ApJ, 701, 824, doi: [10.1088/0004-637X/701/1/824](https://doi.org/10.1088/0004-637X/701/1/824)
- Oates, S. R., & Cummings, J. R. 2009, GRB Coordinates Network, 9265, 1
- Oates, S. R., & Lien, A. Y. 2018, GRB Coordinates Network, 23437, 1
- Oates, S. R., Marshall, F. E., Breeveld, A. A., et al. 2021, MNRAS, 507, 1296, doi: [10.1093/mnras/stab2189](https://doi.org/10.1093/mnras/stab2189)
- O'Connor, B., Beniamini, P., & Kouveliotou, C. 2020, MNRAS, 495, 4782, doi: [10.1093/mnras/staa1433](https://doi.org/10.1093/mnras/staa1433)
- O'Connor, B., Cenko, S. B., Troja, E., et al. 2021, GRB Coordinates Network, 31000, 1
- O'Connor, B., & Troja, E. 2023, GRB Coordinates Network, 33356, 1
- O'Connor, B., Troja, E., Dichiara, S., et al. 2022, MNRAS, 515, 4890, doi: [10.1093/mnras/stac1982](https://doi.org/10.1093/mnras/stac1982)
- Odeh, M. 2022, GRB Coordinates Network, 32968, 1
- Ogawa, F., Adachi, R., Murata, K. L., et al. 2019, GRB Coordinates Network, 26125, 1
- Ohgami, T., Tominaga, N., Utsumi, Y., et al. 2021, PASJ, 73, 350, doi: [10.1093/pasj/pss002](https://doi.org/10.1093/pasj/pss002)

- Olivares, F., Klose, S., Kruehler, T., & Greiner, J. 2009, GRB Coordinates Network, 9352, 1
- Orellana, G., Nagar, N. M., Elbaz, D., et al. 2017, A&A, 602, A68, doi: [10.1051/0004-6361/201629009](https://doi.org/10.1051/0004-6361/201629009)
- Palmese, A., Hartley, W., Tarsitano, F., et al. 2017, ApJL, 849, L34, doi: [10.3847/2041-8213/aa9660](https://doi.org/10.3847/2041-8213/aa9660)
- Pan, Y. C., Sullivan, M., Maguire, K., et al. 2014, MNRAS, 438, 1391, doi: [10.1093/mnras/stt2287](https://doi.org/10.1093/mnras/stt2287)
- Pan, Y. C., Kilpatrick, C. D., Simon, J. D., et al. 2017, ApJL, 848, L30, doi: [10.3847/2041-8213/aa9116](https://doi.org/10.3847/2041-8213/aa9116)
- Panaiteescu, A. 2006, MNRAS, 367, L42, doi: [10.1111/j.1745-3933.2005.00134.x](https://doi.org/10.1111/j.1745-3933.2005.00134.x)
- . 2007, MNRAS, 380, 374, doi: [10.1111/j.1365-2966.2007.12084.x](https://doi.org/10.1111/j.1365-2966.2007.12084.x)
- Panaiteescu, A., Kumar, P., & Narayan, R. 2001, ApJL, 561, L171, doi: [10.1086/324678](https://doi.org/10.1086/324678)
- Pankov, N., Pozanenko, A., Novichonok, A., et al. 2021, GRB Coordinates Network, 29710, 1
- Paspaliaris, E. D., Xilouris, E. M., Nersesian, A., et al. 2023, A&A, 669, A11, doi: [10.1051/0004-6361/202244796](https://doi.org/10.1051/0004-6361/202244796)
- Paterson, K., & Fong, W. 2018, GRB Coordinates Network, 23440, 1
- Paterson, K., Fong, W., Alexander, K. D., Schroeder, G., & Rouco Escorial, A. 2019, GRB Coordinates Network, 26134, 1
- Paterson, K., Fong, W., Nugent, A., et al. 2020, ApJL, 898, L32, doi: [10.3847/2041-8213/aba4b0](https://doi.org/10.3847/2041-8213/aba4b0)
- Paterson, K., Lundquist, M. J., Rastinejad, J. C., et al. 2021, ApJ, 912, 128, doi: [10.3847/1538-4357/abeb71](https://doi.org/10.3847/1538-4357/abeb71)
- Perley, D. A., Bloom, J. S., Modjaz, M., Poznanski, D., & Thoene, C. C. 2007, GRB Coordinates Network, 7140, 1
- Perley, D. A., Zhu, Z. P., Xu, D., et al. 2021, GRB Coordinates Network, 30852, 1
- Perley, D. A., Cenko, S. B., Bloom, J. S., et al. 2009, AJ, 138, 1690, doi: [10.1088/0004-6256/138/6/1690](https://doi.org/10.1088/0004-6256/138/6/1690)
- Perley, D. A., Levan, A. J., Tanvir, N. R., et al. 2013, ApJ, 778, 128, doi: [10.1088/0004-637X/778/2/128](https://doi.org/10.1088/0004-637X/778/2/128)
- Perlmutter, S., Aldering, G., Goldhaber, G., et al. 1999, ApJ, 517, 565, doi: [10.1086/307221](https://doi.org/10.1086/307221)
- Perna, R., & Belczynski, K. 2002, ApJ, 570, 252, doi: [10.1086/339571](https://doi.org/10.1086/339571)
- Piranomonte, S., D'Avanzo, P., Covino, S., et al. 2008, A&A, 491, 183, doi: [10.1051/0004-6361:200810547](https://doi.org/10.1051/0004-6361:200810547)
- Poole, T. S., & La Parola, V. 2006, GRB Coordinates Network, 5068, 1
- Pozanenko, A., Reva, I., Krugov, M., et al. 2021, GRB Coordinates Network, 30972, 1
- Pozanenko, A. S., Minaev, P. Y., Grebenev, S. A., & Chelovekov, I. V. 2020, Astronomy Letters, 45, 710, doi: [10.1134/S1063773719110057](https://doi.org/10.1134/S1063773719110057)
- Rastinejad, J., Paterson, K., Fong, W., et al. 2021a, GRB Coordinates Network, 31002, 1
- . 2021b, GRB Coordinates Network, 29720, 1
- Rastinejad, J. C., Fong, W., Kilpatrick, C. D., Nicholl, M., & Metzger, B. D. 2025, ApJ, 979, 190, doi: [10.3847/1538-4357/ad9c77](https://doi.org/10.3847/1538-4357/ad9c77)
- Rastinejad, J. C., Fong, W., Kilpatrick, C. D., et al. 2021c, ApJ, 916, 89, doi: [10.3847/1538-4357/ac04b4](https://doi.org/10.3847/1538-4357/ac04b4)
- Rastinejad, J. C., Gompertz, B. P., Levan, A. J., et al. 2022a, Nature, 612, 223, doi: [10.1038/s41586-022-05390-w](https://doi.org/10.1038/s41586-022-05390-w)
- Rastinejad, J. C., Paterson, K., Fong, W., et al. 2022b, ApJ, 927, 50, doi: [10.3847/1538-4357/ac4d34](https://doi.org/10.3847/1538-4357/ac4d34)
- Rees, M. J., & Meszaros, P. 1992, MNRAS, 258, 41, doi: [10.1093/mnras/258.1.41P](https://doi.org/10.1093/mnras/258.1.41P)
- Resmi, L., Schulze, S., Ishwara-Chandra, C. H., et al. 2018, ApJ, 867, 57, doi: [10.3847/1538-4357/aae1a6](https://doi.org/10.3847/1538-4357/aae1a6)
- Rhoads, J. E. 1999, ApJ, 525, 737, doi: [10.1086/307907](https://doi.org/10.1086/307907)
- Rhodes, L., Fender, R., Williams, D. R. A., & Mooley, K. 2021, MNRAS, 503, 2966, doi: [10.1093/mnras/stab640](https://doi.org/10.1093/mnras/stab640)
- Riess, A. G., Filippenko, A. V., Challis, P., et al. 1998, AJ, 116, 1009, doi: [10.1086/300499](https://doi.org/10.1086/300499)
- Rigault, M., Brinnel, V., Aldering, G., et al. 2020, A&A, 644, A176, doi: [10.1051/0004-6361/201730404](https://doi.org/10.1051/0004-6361/201730404)
- Rossi, A., Stratta, G., Maiorano, E., Masetti, N., & Palazzi, E. 2020, in Gamma-ray Bursts in the Gravitational Wave Era 2019, ed. T. Sakamoto, M. Serino, & S. Sugita, 106–108
- Rossi, A., Cantiello, M., Testa, V., et al. 2018, GRB Coordinates Network, 22763, 1
- Rossi, A., Palazzi, E., Amati, L., et al. 2021, GRB Coordinates Network, 31107, 1
- Rouco Escorial, A., Fong, W., Veres, P., et al. 2021, ApJ, 912, 95, doi: [10.3847/1538-4357/abee85](https://doi.org/10.3847/1538-4357/abee85)
- Rouco Escorial, A., Fong, W., Berger, E., et al. 2023a, ApJ, 959, 13, doi: [10.3847/1538-4357/acf830](https://doi.org/10.3847/1538-4357/acf830)
- . 2023b, ApJ, 959, 13, doi: [10.3847/1538-4357/acf830](https://doi.org/10.3847/1538-4357/acf830)
- Rumyantsev, V., Antoniuk, K., & Pozanenko, A. 2009, GRB Coordinates Network, 9312, 1
- Saisho, K., Muraki, Y., Ono, Y., et al. 2016, GRB Coordinates Network, 19475, 1
- Saito, Y., Fujiwara, T., Yoshii, T., et al. 2015, GRB Coordinates Network, 18765, 1
- Saito, Y., Tachibana, Y., Yoshii, T., et al. 2016, GRB Coordinates Network, 19495, 1
- Sakamoto, T., Paek, G. S. H., Urata, Y., et al. 2021, GRB Coordinates Network, 31038, 1
- Salafia, O. S., Ghirlanda, G., Ascenzi, S., & Ghisellini, G. 2019, A&A, 628, A18, doi: [10.1051/0004-6361/201935831](https://doi.org/10.1051/0004-6361/201935831)

- Salim, S., Boquien, M., & Lee, J. C. 2018, ApJ, 859, 11, doi: [10.3847/1538-4357/aabf3c](https://doi.org/10.3847/1538-4357/aabf3c)
- Sari, R., & Piran, T. 1995, ApJL, 455, L143, doi: [10.1086/309835](https://doi.org/10.1086/309835)
- Savchenko, V., Ferrigno, C., Kuulkers, E., et al. 2017, ApJL, 848, L15, doi: [10.3847/2041-8213/aa8f94](https://doi.org/10.3847/2041-8213/aa8f94)
- Schady, P. 2018, GRB Coordinates Network, 22662, 1
- Schady, P., & Chen, T. W. 2018, GRB Coordinates Network, 22666, 1
- Schady, P., & Pagani, C. 2006, GRB Coordinates Network, 4877, 1
- Schlafly, E. F., & Finkbeiner, D. P. 2011, ApJ, 737, 103, doi: [10.1088/0004-637X/737/2/103](https://doi.org/10.1088/0004-637X/737/2/103)
- Schmidl, S., Rossi, A., Kann, D. A., & Greiner, J. 2011, GRB Coordinates Network, 12568, 1
- Schneider, B., Le Floc'h, E., Arabsalmani, M., Vergani, S. D., & Palmerio, J. T. 2022, A&A, 666, A14, doi: [10.1051/0004-6361/202243367](https://doi.org/10.1051/0004-6361/202243367)
- Schroeder, G., Fong, W., Berger, E., & Laskar, T. 2023a, GRB Coordinates Network, 33358, 1
- Schroeder, G., Fong, W., Rouco Escorial, A., Laskar, T., & Berger, E. 2021, GRB Coordinates Network, 31021, 1
- Schroeder, G., & Laskar, T. 2023, GRB Coordinates Network, 33372, 1
- Schroeder, G., Laskar, T., & Berger, E. 2023b, GRB Coordinates Network, 33394, 1
- Schroeder, G., Rastinejad, J. C., Fong, W., et al. 2023c, GRB Coordinates Network, 33309, 1
- Schroeder, G., Margalit, B., Fong, W.-f., et al. 2020, ApJ, 902, 82, doi: [10.3847/1538-4357/abb407](https://doi.org/10.3847/1538-4357/abb407)
- Schroeder, G., Laskar, T., Fong, W.-f., et al. 2022, ApJ, 940, 53, doi: [10.3847/1538-4357/ac8feb](https://doi.org/10.3847/1538-4357/ac8feb)
- Schroeder, G., Rhodes, L., Laskar, T., et al. 2024, ApJ, 970, 139, doi: [10.3847/1538-4357/ad49ab](https://doi.org/10.3847/1538-4357/ad49ab)
- Schroeder, G., Fong, W.-f., Kilpatrick, C. D., et al. 2025, ApJ, 982, 42, doi: [10.3847/1538-4357/ada9e5](https://doi.org/10.3847/1538-4357/ada9e5)
- Sezda, S., & Kocevski, D. 2016, GRB Coordinates Network, 19496, 1
- Selsing, J., Vreeswijk, P. M., Japelj, J., et al. 2016, GRB Coordinates Network, 19274, 1
- Shahmoradi, A., & Nemiroff, R. J. 2015, MNRAS, 451, 126, doi: [10.1093/mnras/stv714](https://doi.org/10.1093/mnras/stv714)
- Siegel, M. H., Ambrosi, E., & Swift/UVOT Team. 2023, GRB Coordinates Network, 33289, 1
- Siegel, M. H., Beardmore, A. P., & Swift/UVOT Team. 2020a, GRB Coordinates Network, 28400, 1
- Siegel, M. H., & D'Elia, V. 2018, GRB Coordinates Network, 22665, 1
- Siegel, M. H., & Evans, P. A. 2016, GRB Coordinates Network, 19267, 1
- Siegel, M. H., Groppi, J. D., & Swift/UVOT Team. 2022, GRB Coordinates Network, 31917, 1
- Siegel, M. H., LaPorte, S. J., & Swift/UVOT Team. 2018, GRB Coordinates Network, 22810, 1
- Siegel, M. H., & Lien, A. Y. 2015, GRB Coordinates Network, 18218, 1
- Siegel, M. H., Lien, A. Y., & Swift/UVOT Team. 2020b, GRB Coordinates Network, 27165, 1
- Siegel, M. H., & Mingo, B. 2016, GRB Coordinates Network, 20130, 1
- Siegel, M. H., & Page, K. L. 2016, GRB Coordinates Network, 19291, 1
- Siegel, M. H., Tohuavavohu, A., & Swift/UVOT Team. 2021, GRB Coordinates Network, 30857, 1
- Soderberg, A. M., & Frail, D. A. 2006, GRB Coordinates Network, 4884, 1
- Soderberg, A. M., Frail, D. A., & Chandra, P. 2006a, GRB Coordinates Network, 5388, 1
- Soderberg, A. M., Berger, E., Kasliwal, M., et al. 2006b, ApJ, 650, 261, doi: [10.1086/506429](https://doi.org/10.1086/506429)
- Strausbaugh, R., & Cucchiara, A. 2020a, GRB Coordinates Network, 27792, 1
- . 2020b, GRB Coordinates Network, 27794, 1
- . 2021a, GRB Coordinates Network, 30849, 1
- . 2021b, GRB Coordinates Network, 31214, 1
- . 2023, GRB Coordinates Network, 33286, 1
- Strausbaugh, R., Warshofsky, D., & Kelly, P. L. 2022, GRB Coordinates Network, 32978, 1
- Sullivan, M., Le Borgne, D., Pritchett, C. J., et al. 2006, ApJ, 648, 868, doi: [10.1086/506137](https://doi.org/10.1086/506137)
- Sullivan, M., Conley, A., Howell, D. A., et al. 2010, MNRAS, 406, 782, doi: [10.1111/j.1365-2966.2010.16731.x](https://doi.org/10.1111/j.1365-2966.2010.16731.x)
- Swain, V., Kumar, H., Norboo, R., et al. 2022, GRB Coordinates Network, 32956, 1
- Swift/BAT trigger, T. S. b. s. o. o. t. f. o. G. A. . k. a. t., XRT position, . N. o. a. c. w. t., UVOT photometric system, i. d. i. t. i. U. e. P. -s. u. l. u. t., & exposures are, i. 2023, GRB Coordinates Network, 33370, 1
- Tacchella, S., Conroy, C., Faber, S. M., et al. 2022, ApJ, 926, 134, doi: [10.3847/1538-4357/ac449b](https://doi.org/10.3847/1538-4357/ac449b)
- Tachibana, Y., Fujiwara, T., Yoshii, T., et al. 2016, GRB Coordinates Network, 19130, 1
- Takamatsu, Y., Hosokawa, R., Murata, K. L., et al. 2021, GRB Coordinates Network, 30855, 1
- Tanvir, N. R., Levan, A. J., Fruchter, A. S., et al. 2013, Nature, 500, 547, doi: [10.1038/nature12505](https://doi.org/10.1038/nature12505)
- Tauris, T. M., Kramer, M., Freire, P. C. C., et al. 2017, ApJ, 846, 170, doi: [10.3847/1538-4357/aa7e89](https://doi.org/10.3847/1538-4357/aa7e89)
- Thakur, A. L., Dichiara, S., Troja, E., et al. 2020, MNRAS, 499, 3868, doi: [10.1093/mnras/staa2798](https://doi.org/10.1093/mnras/staa2798)

- Tiurina, N., Lipunov, V., Kornilov, V., et al. 2021, GRB Coordinates Network, 29724, 1
- Torii, K. 2005, GRB Coordinates Network, 3393, 1
- Troja, E., & O'Connor, B. 2023, GRB Coordinates Network, 33360, 1
- Troja, E., Butler, N., Watson, A. M., et al. 2016a, GRB Coordinates Network, 19146, 1
- Troja, E., Watson, A., Covino, S., et al. 2016b, GRB Coordinates Network, 20137, 1
- Troja, E., Butler, N., Watson, A. M., et al. 2017, GRB Coordinates Network, 21051, 1
- Troja, E., Ryan, G., Piro, L., et al. 2018a, *Nature Communications*, 9, 4089, doi: [10.1038/s41467-018-06558-7](https://doi.org/10.1038/s41467-018-06558-7)
- . 2018b, *Nature Communications*, 9, 4089, doi: [10.1038/s41467-018-06558-7](https://doi.org/10.1038/s41467-018-06558-7)
- Troja, E., Butler, N., Watson, A. M., et al. 2018c, GRB Coordinates Network, 22652, 1
- . 2018d, GRB Coordinates Network, 22664, 1
- Troja, E., Fryer, C. L., O'Connor, B., et al. 2022, *Nature*, 612, 228, doi: [10.1038/s41586-022-05327-3](https://doi.org/10.1038/s41586-022-05327-3)
- Tucker, D. L., Wiesner, M. P., Allam, S. S., et al. 2022, *ApJ*, 929, 115, doi: [10.3847/1538-4357/ac5b60](https://doi.org/10.3847/1538-4357/ac5b60)
- Tunnicliffe, R. L., Levan, A. J., Tanvir, N. R., et al. 2014, *MNRAS*, 437, 1495, doi: [10.1093/mnras/stt1975](https://doi.org/10.1093/mnras/stt1975)
- Turpin, D., Adami, C., Le Floc'h, E., et al. 2023, GRB Coordinates Network, 33282, 1
- van der Giessen, S. A., Matsumoto, K., Relano, M., et al. 2024, *A&A*, 692, A39, doi: [10.1051/0004-6361/202451988](https://doi.org/10.1051/0004-6361/202451988)
- van der Hors, A. J. 2006, GRB Coordinates Network, 5408, 1
- van der Horst, A. J. 2005, GRB Coordinates Network, 4039, 1
- van der Horst, A. J., Wiersema, K., & Wijers, R. A. M. J. 2005, GRB Coordinates Network, 3405, 1
- van Paradijs, J., Kouveliotou, C., & Wijers, R. A. M. J. 2000, *ARA&A*, 38, 379, doi: [10.1146/annurev.astro.38.1.379](https://doi.org/10.1146/annurev.astro.38.1.379)
- Varela, K., Knust, F., Bodensteiner, J., & Greiner, J. 2015a, GRB Coordinates Network, 17729, 1
- Varela, K., Knust, F., & Greiner, J. 2015b, GRB Coordinates Network, 17732, 1
- Vergani, S. D., Salvaterra, R., Japelj, J., et al. 2015, *A&A*, 581, A102, doi: [10.1051/0004-6361/201425013](https://doi.org/10.1051/0004-6361/201425013)
- Vieira, N., Ruan, J. J., Haggard, D., et al. 2020, *ApJ*, 895, 96, doi: [10.3847/1538-4357/ab917d](https://doi.org/10.3847/1538-4357/ab917d)
- Vigna-Gómez, A., Neijssel, C. J., Stevenson, S., et al. 2018, *MNRAS*, 481, 4009, doi: [10.1093/mnras/sty2463](https://doi.org/10.1093/mnras/sty2463)
- Volnova, A., Kusakin, A., Moskvitin, A. S., et al. 2017, GRB Coordinates Network, 21419, 1
- Wanderman, D., & Piran, T. 2015, *MNRAS*, 448, 3026, doi: [10.1093/mnras/stv123](https://doi.org/10.1093/mnras/stv123)
- Wang, C. J., Mao, J., & Bai, J. M. 2016, GRB Coordinates Network, 19280, 1
- Wang, F. Y., & Dai, Z. G. 2014, *ApJS*, 213, 15, doi: [10.1088/0067-0049/213/1/15](https://doi.org/10.1088/0067-0049/213/1/15)
- Wang, J., Fu, J., Aumer, M., et al. 2014, *MNRAS*, 441, 2159, doi: [10.1093/mnras/stu649](https://doi.org/10.1093/mnras/stu649)
- Watson, A. M., Butler, N., Becerra, R. L., et al. 2018, GRB Coordinates Network, 23089, 1
- Watson, A. M., Butler, N. R., Lee, W. H., et al. 2020, *MNRAS*, 492, 5916, doi: [10.1093/mnras/staa161](https://doi.org/10.1093/mnras/staa161)
- Watson, A. M., Troja, E., Butler, N., et al. 2021a, GRB Coordinates Network, 30534, 1
- Watson, A. M., Butler, N., Kutyrev, A., et al. 2021b, GRB Coordinates Network, 30973, 1
- Wieringa, M. H., Chandra, P., & Frail, D. A. 2007, GRB Coordinates Network, 7095, 1
- Williams, G. G., & Milne, P. A. 2008, GRB Coordinates Network, 8400, 1
- Wiseman, P., Bolmer, J., & Greiner, J. 2016, GRB Coordinates Network, 19959, 1
- Wu, Y., & MacFadyen, A. 2019, *ApJL*, 880, L23, doi: [10.3847/2041-8213/ab2fd4](https://doi.org/10.3847/2041-8213/ab2fd4)
- Xu, D., Zhu, Z. P., Fu, S. Y., et al. 2020, GRB Coordinates Network, 29118, 1
- Xu, D., Qin, Y., Zhao, Y., et al. 2017, GRB Coordinates Network, 21048, 1
- Yang, B., Jin, Z.-P., Li, X., et al. 2015, *Nature Communications*, 6, 7323, doi: [10.1038/ncomms8323](https://doi.org/10.1038/ncomms8323)
- Yang, J., Ai, S., Zhang, B.-B., et al. 2022, *Nature*, 612, 232, doi: [10.1038/s41586-022-05403-8](https://doi.org/10.1038/s41586-022-05403-8)
- Yang, Y.-H., Troja, E., O'Connor, B., et al. 2024, *Nature*, 626, 742, doi: [10.1038/s41586-023-06979-5](https://doi.org/10.1038/s41586-023-06979-5)
- Yates, R., Chen, T. W., & Greiner, J. 2016a, GRB Coordinates Network, 19292, 1
- Yates, R., Kruehler, T., & Greiner, J. 2016b, GRB Coordinates Network, 19272, 1
- Yi, W. M., Mao, J., & Bai, J. M. 2016, GRB Coordinates Network, 19270, 1
- Yoshida, M., Kuroda, D., Yanagisawa, K., et al. 2009a, GRB Coordinates Network, 9266, 1
- . 2009b, GRB Coordinates Network, 9267, 1
- Yost, S. A., Harrison, F. A., Sari, R., & Frail, D. A. 2003, *ApJ*, 597, 459, doi: [10.1086/378288](https://doi.org/10.1086/378288)
- Zevin, M., Nugent, A. E., Adhikari, S., et al. 2022, *ApJL*, 940, L18, doi: [10.3847/2041-8213/ac91cd](https://doi.org/10.3847/2041-8213/ac91cd)
- Zhang, B., Zhang, B.-B., Virgili, F. J., et al. 2009, *ApJ*, 703, 1696, doi: [10.1088/0004-637X/703/2/1696](https://doi.org/10.1088/0004-637X/703/2/1696)

- Zhang, B. B., Liu, Z. K., Peng, Z. K., et al. 2021, Nature Astronomy, 5, 911, doi: [10.1038/s41550-021-01395-z](https://doi.org/10.1038/s41550-021-01395-z)
- Zhao, W., Zhang, J.-C., Zhang, Q.-X., et al. 2020, ApJ, 900, 112, doi: [10.3847/1538-4357/aba43a](https://doi.org/10.3847/1538-4357/aba43a)
- Zheng, W., Filippenko, A. V., & KAIT GRB Team. 2021, GRB Coordinates Network, 31203, 1
- Zhou, H., Jin, Z.-P., Covino, S., et al. 2023, ApJ, 943, 104, doi: [10.3847/1538-4357/acac9b](https://doi.org/10.3847/1538-4357/acac9b)
- Ziaeepour, H., Baumgartner, W., Cummings, J., et al. 2008, GCN Report

## APPENDIX

## A. SAMPLE SIZE

Here, we show a table that list the  $\gamma$ -ray  $T_{90}$  of each short GRB in our sample, along with its bands in which afterglow follow-up was pursued. We also include the references where we collected the afterglow observations.

**Table A1.** Wavelength Availability

GRB	$T_{90}$	X-ray	Optical	Radio	References
050202	0.27	N	Y	Y <sup>a</sup>	Castro-Tirado et al. (2005); Frail & Soderberg (2005)
050509B	0.024	Y	Y	Y	Torii (2005); van der Horst et al. (2005)
050709 <sup>b</sup>	0.07	Y	Y	Y	Fox et al. (2005)
050724A <sup>b</sup>	98.0	Y	Y	Y	Berger et al. (2005); Panaiteescu (2006); Malesani et al. (2007b)
050813	0.38	Y	Y	Y	Blustin et al. (2005b); Cameron & Frail (2005a); Fox & Cenko (2005)
050906	0.26	N	Y	Y	Cameron & Frail (2005b); Levan et al. (2008)
050925	...	N	N	Y	van der Horst (2005)
051105A	...	N	N	Y	Frail & Cameron (2005)
051114A	...	N	N	Y <sup>a</sup>	Frail (2005)
051210	1.3	Y	Y	N	Blustin et al. (2005a)
051221A	1.4	Y	Y	Y	Soderberg et al. (2006b)
060121	2.0	Y	Y	N	Levan et al. (2006)
060313	0.74	Y	Y	Y <sup>a</sup>	Schady & Pagani (2006); Soderberg & Frail (2006)
060502B	0.09	N	Y	N	Poole & La Parola (2006)
060614 <sup>a,b</sup>	102.0	Y	Y	Y	Rastinejad et al. (2021c)
060801	0.5	Y	Y	Y	Brown & Racusin (2006); Soderberg et al. (2006a); van der Hors (2006)
061006	129.9	Y	Y	N	D'Avanzo et al. (2009)
061201	0.8	Y	Y	N	Holland & Marshall (2006)
061210	85.3	Y	Y	Y <sup>a</sup>	Cenko et al. (2006); Chandra & Frail (2006)
061217	0.2	N	Y	N	Berger et al. (2007)
070209	0.09	N	Y	N	Johnson et al. (2007)
070406	1.2	N	Y	N	Malesani et al. (2007a)
070429B	0.5	Y	Y	Y <sup>a</sup>	Chandra & Frail (2007a); Nysewander et al. (2007); Perley et al. (2007)
070707	1.1	N	Y	N	Piranomonte et al. (2008)
070714B <sup>b</sup>	64.0	Y	Y	Y <sup>a</sup>	Chandra & Frail (2007b); Graham et al. (2009)
070724A	0.4	Y	Y	Y <sup>a</sup>	Chandra & Frail (2007c); Berger et al. (2009)
070729	0.9	Y	Y	Y <sup>a</sup>	Chandra & Frail (2007d); Fong et al. (2015)
070809 <sup>b</sup>	1.3	Y	Y	N	Fong et al. (2015)
070810B	0.08	N	Y	N	Fong et al. (2015)
070923	...	N	N	Y <sup>a</sup>	Chandra & Frail (2007e)
071112B	0.3	N	Y	Y <sup>a</sup>	Wieringa et al. (2007); Fong et al. (2015)
071227	142.5	Y	Y	N	Fong et al. (2015)
080121	0.7	N	Y	N	Fong et al. (2015)
080123	115.0	Y	Y	N	Cucchiara & Ukwatta (2008); Fong et al. (2015)
080426	1.7	Y	Y	N	Ziaeepour et al. (2008); Fong et al. (2015)

**Table A1** *continued*

**Table A1** (*continued*)

GRB	$T_{90}$	X-ray	Optical	Radio	References
080503 <sup>b</sup>	170.0	Y	Y	Y	Frail & Chandra (2008); Kuroda et al. (2008); Fong et al. (2015)
080702A	0.5	Y	Y	Y <sup>a</sup>	Chandra & Frail (2008a); de Pasquale (2008); Mori et al. (2008); Fong et al. (2015)
080905A	1.0	Y	Y	N	Brown & Pagani (2008); Nakajima et al. (2008); Fong et al. (2015)
080919	0.6	Y	Y	N	Immler & Holland (2008); Fong et al. (2015)
081024A	1.8	Y	Y	Y <sup>a</sup>	Chandra & Frail (2008b); de Pasquale & Stratta (2008); Melandri et al. (2008); Williams & Milne (2008); Fong et al. (2015)
081024B	1.8	N	Y	Y <sup>a</sup>	Chandra et al. (2008); Fong et al. (2015)
081226A	0.4	Y	Y	Y <sup>a</sup>	Hoversten & Godet (2008); Moin et al. (2009b); Fong et al. (2015)
081226B	0.4	N	Y	Y <sup>a</sup>	Moin et al. (2009c); Fong et al. (2015)
090305	0.54	N	Y	N	Fong et al. (2015)
090417A	...	N	N	Y	Chandra & Frail (2009)
090426	1.2	Y	Y	N	Kinugasa et al. (2009); Oates & Cummings (2009); Rumyantsev et al. (2009); Yoshida et al. (2009b,a); Fong et al. (2015)
090510	5.66	Y	Y	Y	Frail & Chandra (2009); Kuin & Hoversten (2009); Olivares et al. (2009); Fong et al. (2015)
090515	0.036	Y	Y	Y	Berger & Fong (2009b); Fong et al. (2015)
090607	2.3	Y	Y	N	Fong et al. (2015)
090621B	0.14	Y	Y	Y	Berger & Fong (2009c); Fong et al. (2015)
090715A	...	N	N	Y	Berger & Fong (2009d)
090916	0.3	N	Y	N	Fong et al. (2015)
090927A	...	N	N	Y <sup>a</sup>	Moin et al. (2009a)
091109B	0.3	Y	Y	N	Fong et al. (2015)
091117	0.43	N	Y	Y <sup>a</sup>	Berger & Fong (2009a); Fong et al. (2015)
100117A	0.291	Y	Y	N	Fong et al. (2015)
100206A	0.12	Y	Y	N	Fong et al. (2015)
100213A	...	Y	N	N	Evans et al. (2007, 2009)
100625A	0.33	Y	Y	Y <sup>a</sup>	Fong et al. (2015)
100628A	0.036	N	Y	Y <sup>a</sup>	Fong et al. (2015)
100702A	0.16	Y	Y	N	Fong et al. (2015)
101219A	0.827	Y	Y	N	Fong et al. (2015)
101224A	...	Y	N	Y	Fong et al. (2015)
110112A	0.524	Y	Y	Y	Fong et al. (2015)
110112B	0.524	N	Y	Y	Fong et al. (2015)
110420B	0.08	N	Y	Y	Fong et al. (2015)
111020A	0.384	Y	Y	Y	Fong et al. (2012, 2015)
111117A	0.47	Y	Y	Y	Schmidl et al. (2011); Margutti et al. (2012)
111121A	...	Y	N	Y <sup>a</sup>	Fong et al. (2015)
120229A	0.22	N	Y	Y	Fong et al. (2015)
120305A	0.1	Y	Y	Y	Fong et al. (2015)
120521A	0.45	Y	Y	Y	Hancock et al. (2012a); Fong et al. (2015)
120804A	0.81	Y	Y	Y	Fong et al. (2015); Berger et al. (2013b); Hancock et al. (2012b)
120817B	0.19	N	Y	N	Fong et al. (2015)
121226A	1.0	Y	Y	Y	Fong et al. (2015)
130313A	0.26	N	Y	Y	Fong et al. (2015)
130515A	0.29	Y	Y	N	Fong et al. (2015)

**Table A1** *continued*

**Table A1** (*continued*)

GRB	$T_{90}$	X-ray	Optical	Radio	References
130603B <sup>b</sup>	0.18	Y	Y	Y	Fong et al. (2014, 2015)
130716A	87.7	Y	Y	Y	Fong et al. (2015)
130822A	0.04	Y	Y	Y	Fong et al. (2015)
130912A	0.28	Y	Y	Y	Fong et al. (2015)
131004A	1.54	Y	Y	Y <sup>a</sup>	Fong et al. (2015)
131125A	0.5	N	Y	N	Fong et al. (2015)
131126A	0.3	N	Y	N	Fong et al. (2015)
131224A	...	N	N	Y	Fong et al. (2015)
140129B	1.36	Y	Y	N	Fong et al. (2015)
140320A	0.45	Y	Y	N	Fong et al. (2015)
140402A	0.03	N	Y	N	Fong et al. (2015)
140414A	0.7	N	Y	N	Fong et al. (2015)
140516A	0.19	Y	Y	Y	Fong et al. (2015)
140606A	0.34	N	Y	N	Fong et al. (2015)
140619B	0.5	N	Y	Y	Fong et al. (2015)
140622A	0.13	Y	Y	Y	Fong et al. (2015)
140903A	0.29	Y	Y	Y	Fong et al. (2015)
140930B	0.84	Y	Y	Y	Fong et al. (2015)
141205A	1.1	N	Y	N	Fong et al. (2015)
141212A	0.3	Y	Y	Y	Fong et al. (2015)
150101B <sup>b</sup>	0.018	Y	Y	Y <sup>a</sup>	Fong et al. (2015, 2016)
150101A	...	Y	N	Y	Fong et al. (2015)
150120A	1.2	Y	Y	Y	Fong et al. (2015)
150423A	0.22	Y	Y	N	Harita et al. (2015); Kuroda et al. (2015a); Littlejohns et al. (2015); Marshall & Pagani (2015); Mazaeva et al. (2015b); Varela et al. (2015a,b)
150424A	0.5	Y	Y	Y	Butler et al. (2015); Kann et al. (2015); Marshall & Beardmore (2015); Fong et al. (2021)
150728A	0.8	Y	Y	N	Breeveld & Krimm (2015); Mazaeva et al. (2015a)
150831A	1.15	Y	Y	N	Knust et al. (2015); Siegel & Lien (2015)
151229A	1.44	Y	Y	N	de Pasquale & Kocevski (2015); Kuroda et al. (2015b); Saito et al. (2015)
160303A	5.0	Y	Y	N	Butler et al. (2016); Elenin et al. (2016); Emery & Beardmore (2016); Fong (2016); Graham et al. (2016); Jeong et al. (2016a); Kuroda et al. (2016a); Klose et al. (2016); Tachibana et al. (2016); Troja et al. (2016a)
160408A	0.32	Y	Y	N	Siegel & Evans (2016); Yi et al. (2016)
160410A	96.0	Y	Y	N	Malesani et al. (2016); Marshall & Gibson (2016); Muraki et al. (2016); Selsing et al. (2016); Wang et al. (2016); Yates et al. (2016b); Agüí Fernández et al. (2023)
160411A	0.36	Y	Y	N	Siegel & Page (2016); Yates et al. (2016a)
160525B	0.29	Y	Y	N	de Pasquale et al. (2016); Saisho et al. (2016); O'Connor et al. (2022)
160601A	0.12	Y	Y	N	Kuroda et al. (2016b); Saito et al. (2016); Sebzda & Kocevski (2016)
160624A	0.192	Y	Y	N	de Pasquale & D'Ai (2016); Kuroda et al. (2016c)
160821B <sup>b</sup>	0.48	Y	Y	Y	Breeveld & Siegel (2016); Jeong et al. (2016b); Lamb et al. (2019b); Fong et al. (2021)
160927A	0.48	Y	Y	N	Kuin & Gibson (2016); Wiseman et al. (2016)
161001A	2.6	Y	Y	N	Chen et al. (2016); Kuin & Page (2016); Murata et al. (2016)
161104A	0.1	Y	Y	N	Siegel & Mingo (2016); Troja et al. (2016b); Nugent et al. (2020)
170127B	0.51	Y	Y	Y	Cano et al. (2017); Marshall & Cannizzo (2017)

**Table A1** *continued*

**Table A1** (*continued*)

GRB	$T_{90}$	X-ray	Optical	Radio	References
170325A	...	N	N	Y	Mooley et al. (2017a)
170428A	0.2	Y	Y	Y	Bolmer et al. (2017); D'Avanzo et al. (2017); Kuin & Beardmore (2017); Mooley et al. (2017b); Troja et al. (2017); Xu et al. (2017)
170524A	...	N	N	Y	Mooley et al. (2017c)
170728A	1.25	Y	Y	Y <sup>a</sup>	Cucchiara et al. (2017); Laporte & Cannizzo (2017); Mooley et al. (2017e)
170728B	47.7	Y	Y	Y	Chandra & Nayana (2017); Fong et al. (2017); Heintz et al. (2017); Laporte & Cenko (2017); Laporte (2017); Mooley et al. (2017d); Volnova et al. (2017)
170817	2.64	N	Y	N	Blanchard et al. (2017); Rossi et al. (2018)
180402A	0.18	Y	Y	N	Butler et al. (2018); Emery & Lien (2018)
180418A	1.9	Y	Y	N	Choi et al. (2018); Fong et al. (2018b); Guidorzi et al. (2018b); Horiuchi et al. (2018); Malesani et al. (2018); Rouco Escorial et al. (2021); Schady (2018); Schady & Chen (2018); Siegel & D'Elia (2018); Troja et al. (2018c,d)
180618A	47.4	Y	Y	N	Guidorzi et al. (2018a); Mazaeva et al. (2018); Siegel et al. (2018)
180727A	1.06	Y	Y	N	Marshall & Beardmore (2018)
180805B	122.5	Y	Y	N	Higgins et al. (2018); Kuin & D'Avanzo (2018); Watson et al. (2018)
181123B	0.26	Y	Y	Y	Anderson et al. (2018); Fong et al. (2018a); Oates & Lien (2018); Paterson & Fong (2018); Paterson et al. (2020)
191031D	0.29	Y	Y	Y	Butler et al. (2019); Dichiara & Troja (2019); Gropp et al. (2019); Laskar et al. (2019); Ogawa et al. (2019); Paterson et al. (2019)
200219A	0.5	Y	Y	Y	d'Antonio et al. (2020); Siegel et al. (2020b)
200411A	0.22	Y	Y	Y	Anderson et al. (2020); Kuin et al. (2020b); Lipunov et al. (2020a)
200522A <sup>b</sup>	0.616	Y	Y	Y	Dichiara et al. (2020b); Hu et al. (2020); Kuin et al. (2020a); Lipunov et al. (2020c); Strausbaugh & Cucchiara (2020a,b); Fong et al. (2021)
200907B	0.83	Y	Y	N	Siegel et al. (2020a)
201006A	0.49	Y	Y	Y	Dichiara et al. (2020a); Ito et al. (2020); Marshall et al. (2020); Schroeder et al. (2025)
201221D	0.16	Y	Y	N	Breeveld et al. (2020); Dichiara et al. (2020c); Dimple et al. (2020); Lipunov et al. (2020b); Malesani & Knudstrup (2020); Xu et al. (2020)
210323A	1.12	Y	Y	Y	Breeveld et al. (2021); de Ugarte Postigo et al. (2021a); Fu et al. (2021); Malesani et al. (2021a); Pankov et al. (2021); Rastinejad et al. (2021b); Tiurina et al. (2021); Schroeder et al. (2025)
210726A	0.38	Y	Y	Y	Watson et al. (2021a); Schroeder et al. (2024)
210919A	0.16	Y	Y	Y	Kim et al. (2021); Perley et al. (2021); Siegel et al. (2021); Kann et al. (2021); Takamatsu et al. (2021)
211023B	1.3	Y	Y	Y	Grossan et al. (2021); Hosokawa et al. (2021); Hu et al. (2021); Kuin et al. (2021); Kuin et al. (2021); O'Connor et al. (2021); Pozanenko et al. (2021); Rastinejad et al. (2021a); Rossi et al. (2021); Sakamoto et al. (2021); Schroeder et al. (2021); Watson et al. (2021b)
211106A	1.75	Y	Y	Y	de Wet et al. (2021a); Nicuesa Guelbenzu et al. (2021); Laskar et al. (2022)
211211A <sup>b</sup>	51.37	Y	Y	Y	Belles et al. (2021); de Ugarte Postigo et al. (2021b); Ito et al. (2021); Jiang et al. (2021); Kumar et al. (2021); Levan et al. (2021); Lipunov et al. (2021); Malesani et al. (2021b); Strausbaugh & Cucchiara (2021b); Zheng et al. (2021); Rastinejad et al. (2022a)
220412B	...	N	Y	N	D'Avanzo et al. (2022); Kumar et al. (2022); Murata et al. (2022); Siegel et al. (2022)
220730A	...	N	Y	N	Kuin et al. (2022a)
220831A	...	N	N	Y	Anderson et al. (2022)
221120A	...	N	Y	N	Gompertz et al. (2022); Kuin et al. (2022b); Odeh (2022); Strausbaugh et al. (2022); Swain et al. (2022)
230205A	...	Y	Y	Y	Schroeder et al. (2023c); Schroeder & Laskar (2023); Siegel et al. (2023); Strausbaugh & Cucchiara (2023); Turpin et al. (2023)
230217A	...	Y	Y	Y	Anderson et al. (2023); Capalbi et al. (2023); D'Avanzo et al. (2023); O'Connor & Troja (2023);

**Table A1** *continued*

**Table A1** (*continued*)

GRB	$T_{90}$	X-ray	Optical	Radio	References
					Schroeder et al. (2023a); Swift/BAT trigger et al. (2023); Troja & O'Connor (2023)
230228A	...	Y	Y	Y	Belkin et al. (2023); Breeveld et al. (2023); Evans & Swift-XRT Team (2023); Hu et al. (2023); Komesh et al. (2023); Lu et al. (2023); Noonan et al. (2023); Schroeder et al. (2023b)
230307A <sup>b</sup>	33.0	Y	Y	Y	Burns et al. (2023); Casentini et al. (2023)
231117A	0.668	Y	Y	Y	Schroeder et al. (2025)

NOTE—The  $T_{90}$  and presence of an X-ray, optical, and radio afterglow observation for the 151 short GRBs within our sample. Here, “Y” denotes an observation (detection or upper limit), “N” denotes the absence of one. Refer to Evans et al. (2007, 2009); Fong et al. (2015); Rouco Escorial et al. (2023a) for the X-ray afterglow sample.

<sup>a</sup>Shallow radio follow up ( $> 100 \mu\text{Jy}$ )

<sup>b</sup>GRBs with possible KNe affecting their optical afterglow. We give the time intervals here for which KN emission may dominate, and avoid these time ranges in our analysis: GRB 050709:  $\delta t \approx 1 - 4$  days (Gompertz et al. 2018; Rossi et al. 2020; Rastinejad et al. 2021c); GRB 050724A:  $\delta t \approx 1.45 - 3.46$  days (Rossi et al. 2020; Rastinejad et al. 2021c); GRB 060614:  $\delta t \approx 3.86 - 7.84$  days (Gompertz et al. 2018; Rossi et al. 2020; Rastinejad et al. 2021c; Jin et al. 2015; Yang et al. 2015); GRB 070714B:  $\delta t \approx 1 - 1.03$  days (Rossi et al. 2020; Rastinejad et al. 2021c); GRB 070809:  $\delta t \approx 0.47 - 1.46$  days (Rossi et al. 2020; Rastinejad et al. 2021c; Jin et al. 2020); GRB 080503:  $\delta t \approx 0.04 - 5.36$  days (Rastinejad et al. 2021c; Zhou et al. 2023); GRB 130603B:  $\delta t \approx 9.37 - 9.49$  days (Gompertz et al. 2018; Rossi et al. 2020; Rastinejad et al. 2021c; Berger et al. 2013a; Tanvir et al. 2013); GRB 150101B:  $\delta t \approx 1.66 - 10.71$  days (Rossi et al. 2020; Rastinejad et al. 2021c; Fong et al. 2016; Troja et al. 2018a); GRB 160821B:  $\delta t \approx 1.06 - 10.53$  days (Rossi et al. 2020; Rastinejad et al. 2021c; Kasliwal et al. 2017; Lamb et al. 2019b); GRB 200522A:  $\delta t \approx 3.12 - 3.66$  days (Rossi et al. 2020; O'Connor et al. 2022); GRB 211211A:  $\delta t \approx 0.3 - 5$  days (Rastinejad et al. 2022a; Troja et al. 2022; Yang et al. 2022); GRB 230307A:  $\delta t \approx 1 - 61$  days (Gillanders et al. 2023; Levan et al. 2024; Yang et al. 2024). For GRB 211211A, we use an afterglow model from Rastinejad et al. (2025) to estimate the afterglow contribution.

## B. X-RAY AND OPTICAL $L_C$ WITH ENVIRONMENTAL PROPERTIES

We present a table showing our determined X-ray and optical luminosities at a common rest-frame time of  $\delta t_c = 3$  hr ( $L_c$ ) for each GRB (see Section 3), along with its environmental properties from the Broadband Repository for Investigating Gamma-ray burst Host Traits (BRIGHT<sup>8</sup>; Fong et al. 2022; Nugent et al. 2022) and from Levan et al. (2024); Schroeder et al. (2025); Nugent et al. (2025). Optical  $L_{cs}$  without  $\sigma_{L_{C\,\text{opt}}}$  represent the deepest upper limit within 2.5 hr from  $\delta t_c$ .

<sup>8</sup> <http://bright.ciera.northwestern.edu>

**Table B2.** Afterglow Luminosities at a Common Rest-frame Time of 3 hr and Environmental Properties

GRB	z	$\log(L_{C,\text{opt}})$	$\log(\sigma_{L_{C,\text{opt}}})$	$\log(L_{C,\text{X}})$	$\log(\sigma_{L_{C,\text{X}}})$	$\log(M_*/M_\odot)$	SFR	$\log(s\text{SFR})$	$\log(s\text{SFR})$	$\delta R_{\text{phys}}$	$\delta R_{\text{norm}}$	$A_V, \text{host}$	$t_m$
		[erg/s]	[erg/s]	[erg/s]	[erg/s]	[erg/s]	[ $M_\odot \text{ yr}^{-1}$ ]	[ $\text{yr}^{-1}$ ]	[kpc]	[ $r_e$ ]	[mag]	[Gyr]	
050509B	0.225	< 41.745	...	41.827	41.128	11.46	0.21	-12.138	55.19	2.59	...	8.84	
050709	0.161	42.91	42.09	44.464	43.765	8.55	0.02	-10.249	3.76	2.0	0.02	0.57	
050724A	0.254	43.74	42.91	44.094	43.395	11.05	0.15	-11.874	2.74	0.67	0.76	8.20	
050813	0.719	...	...	42.209	41.51	10.31	1.53	-10.125	43.57	...	0.23	3.73	
051210	0.64	...	...	44.125	43.426	10.96	434.96	-8.322	29.08	5.65	1.9	0.23	
051221A	0.546	43.977	43.274	45.325	44.626	9.31	0.71	-9.459	2.08	0.89	0.32	0.49	
060121	0.64	43.15	42.412	45.689	44.99	...	...	...	0.97	0.18	...	...	
060313	0.64	43.969	43.453	45.296	44.597	...	...	...	2.6	1.39	...	...	
060502B	1.51	46.585	44.637	...	...	...	...	...	...	...	...	...	
060614	0.125	41.65	41.89	44.63	43.94	7.85	0.004	-10.25	0.7	0.86	0.1	0.76	
060801	1.13	...	...	44.377	43.678	9.12	9.18	-8.157	10.25	...	0.3	0.13	
061006	0.461	43.91	43.086	44.389	43.69	9.37	0.1	-10.37	1.39	0.37	0.24	4.27	
061201	0.64	43.397	42.573	45.199	44.5	...	...	...	33.09	14.91	...	...	
061210	0.41	< 42.738	...	44.939	44.241	9.77	0.19	-10.491	15.51	...	0.3	0.66	
061217	0.827	< 43.515	...	...	...	...	...	...	...	...	...	...	
070429B	0.902	< 43.711	...	44.324	43.625	10.44	8.66	-9.502	6.0	1.17	2.0	0.43	
070507	0.64	43.727	42.898	...	...	...	...	...	3.25	1.11	...	...	
070714B	0.923	44.601	43.384	44.884	44.185	9.37	1.23	-9.28	12.33	5.17	0.33	1.63	
070724A	0.457	42.603	41.779	44.478	43.779	9.81	6.48	-8.998	5.52	1.49	1.25	0.27	
070729	0.52	...	...	43.744	43.045	8.76	0.89	-8.811	19.72	...	0.31	0.55	
070809	0.473	43.20	42.37	44.791	44.092	10.82	0.83	-10.901	34.11	9.34	1.05	0.84	
071112B	0.64	< 43.241	...	...	...	...	...	...	...	...	...	...	
071227	0.381	43.145	42.321	43.791	43.092	10.79	5.8	-10.027	14.74	3.08	1.45	1.79	
080123	0.495	...	...	43.798	43.099	10.12	9.3	-9.152	53.63	...	0.62	0.43	
080426	1.7	< 44.575	...	45.531	44.832	...	...	...	...	...	...	...	
080503	0.64	...	...	43.887	43.188	...	...	...	7.31	3.46	...	...	
080702A	0.64	...	...	41.033	44.099	...	...	...	...	...	...	...	
080905A	0.1218	41.211	40.387	43.536	42.837	...	...	...	18.3	4.61	...	...	
080919	0.64	46.05	45.226	43.778	43.079	...	...	...	...	...	...	...	
081024A	0.64	< 44.829	...	43.872	43.173	...	...	...	...	...	...	...	
081226A	0.64	42.714	41.89	43.293	42.594	...	...	...	...	...	...	...	

Table B2 *continued*

**Table B2** (*continued*)

GRB	z	$\log(L_{C,\text{opt}})$	$\log(\sigma_{L_{C,\text{opt}}})$	$\log(L_{C,\text{X}})$	$\log(\sigma_{L_{C,\text{X}}})$	$\log(M_*/M_\odot)$	SFR	$\log(\text{sSFR})$	$\delta R_{\text{phys}}$	$\delta R_{\text{nrm}}$	$A_V, \text{host}$	$t_m$
		[erg/s]	[erg/s]	[erg/s]	[erg/s]	[erg/s]	[ $M_\odot \text{ yr}^{-1}$ ]	[yr $^{-1}$ ]	[kpc]	[ $r_e$ ]	[mag]	[Gyr]
090305	0.64	42.892	41.446	...	...	...	...	...	...	...	...	...
090426	2.609	46.041	43.604	46.029	45.33	...	...	0.49	0.29	...	...	...
090510	0.903	43.975	43.481	44.914	44.215	9.75	1.26	-9.65	10.51	1.66	0.54	0.45
090515	0.403	41.511	40.688	43.388	42.689	11.25	...	...	76.19	13.98	0.1	6.34
090607	0.64	...	...	43.402	42.703	...	...	...	...	...	...	...
090621B	0.64	...	...	44.588	43.889	...	...	...	...	...	...	...
090916	0.64	< 44.794	...	...	...	...	...	...	...	...	...	...
091109B	0.64	42.81	41.986	44.542	43.843	...	...	...	4.22	1.93	...	...
100117A	0.914	42.918	42.094	44.043	43.344	10.35	...	...	1.35	0.61	0.16	3.02
100206A	0.407	...	...	42.697	41.998	10.72	7.64	-9.837	25.28	...	1.19	4.58
100213A	0.64	...	...	44.208	43.509	...	...	...	...	...	...	...
100625A	0.452	...	...	42.816	42.117	9.7	...	...	2.63	...	0.1	3.56
100628A	0.64	< 42.785	...	...	...	...	...	...	...	...	...	...
100702A	0.64	< 43.232	...	44.609	43.91	...	...	...	...	...	...	...
101219A	0.718	< 42.986	...	42.215	44.00	9.39	3.14	-8.893	5.48	...	1.5	0.25
101224A	0.454	...	...	43.904	43.205	9.17	0.58	-9.407	12.75	...	0.2	0.46
110112A	0.64	43.798	42.974	44.592	43.893	...	...	...	18.03	6.53	...	...
111020A	0.64	...	...	45.154	44.455	...	...	...	...	...	...	...
111117A	2.211	< 44.268	...	45.019	44.32	9.63	22.11	-8.285	10.52	...	0.3	0.19
111121A	0.64	...	...	45.452	44.753	...	...	...	...	...	...	...
120305A	0.225	...	...	43.1	42.401	9.17	0.03	-10.693	18.09	...	0.02	2.11
120521A	0.64	...	...	44.686	43.987	...	...	...	...	...	...	...
120804A	1.05	43.319	42.495	45.781	45.082	9.81	18.79	-8.536	2.22	...	2.77	0.35
121226A	1.37	< 44.436	...	45.706	45.007	9.46	24.59	-8.069	2.31	...	1.01	0.12
130313A	2.79	< 44.161	...	...	...	...	...	...	...	...	...	...
130515A	0.8	...	...	43.979	43.28	10.28	0.26	-10.865	61.22	...	0.14	0.78
130603B	0.357	43.803	43.044	45.236	44.537	9.82	0.44	-10.177	5.4	0.71	0.29	1.63
130716A	2.2	...	...	44.832	44.133	9.61	11.99	-8.531	33.08	...	0.4	0.32
130822A	0.154	...	...	41.754	41.055	10.16	0.3	-10.683	60.09	...	0.21	2.16
130912A	0.64	43.66	42.835	45.127	44.428	...	...	...	3.9	1.41	...	...
131004A	0.717	44.134	43.477	45.005	44.306	...	...	...	0.8	0.25	...	...
140129B	0.43	45.513	43.384	44.769	44.07	9.33	0.06	-10.552	1.76	...	0.09	1.65
140320A	0.64	...	...	47.081	46.382	...	...	...	...	...	...	...

**Table B2** (*continued*)

**Table B2** (*continued*)

GRB	z	$\log(L_{C,\text{opt}})$	$\log(\sigma_{L_{C,\text{opt}}})$	$\log(L_{C,\text{X}})$	$\log(\sigma_{L_{C,\text{X}}})$	$\log(M_*/M_\odot)$	SFR	$\log(s\text{SFR})$	$\delta R_{\text{phys}}$	$\delta R_{\text{norm}}$	$A_V, \text{host}$	$t_m$
		[erg/s]	[erg/s]	[erg/s]	[erg/s]	[M $_\odot$ yr $^{-1}$ ]	[yr $^{-1}$ ]	[kpc]	[r $_e$ ]	[mag]	[Gyr]	
140516A	1.47	< 43.533	...	43.606	42.907	...	...	...	...	...	...	...
140606A	0.64	< 43.75	...	...	...	...	...	...	...	...	...	...
140622A	0.959	...	...	43.404	42.705	10.17	6.01	-9.391	32.95	...	0.61	0.66
140903A	0.353	44.733	43.909	45.409	44.71	10.81	2.28	-10.452	0.9	...	2.99	4.24
140930B	1.465	44.104	43.28	45.325	44.626	9.45	5.13	-8.74	9.62	...	0.28	0.57
141212A	0.596	< 43.942	...	43.979	43.28	9.71	1.17	-9.642	18.75	...	0.43	2.37
150101A	0.64	...	...	43.285	42.586	...	...	...	...	...	...	...
150101B	0.134	...	...	44.409	43.71	11.13	0.22	-11.788	7.36	0.78	0.25	4.88
150120A	0.4604	< 42.021	...	43.915	43.216	10.01	2.27	-9.654	4.77	...	1.1	2.28
150423A	1.394	43.664	42.365	43.429	42.73	...	...	...	...	...	...	...
150424A	0.64	43.449	42.625	45.812	45.113	...	...	...	3.41	1.5	...	...
150728A	0.461	...	...	44.754	44.055	9.35	8.13	-8.44	7.52	...	0.86	9.35
150831A	1.18	...	...	45.014	44.315	9.49	5.97	-8.714	12.43	...	1.02	0.51
151229A	0.63	< 45.23	...	46.168	45.469	8.79	0.22	-9.448	8.16	...	0.87	1.78
160303A	1.01	43.891	43.127	45.152	44.453	9.51	2.37	-9.135	15.31	3.42	1.61	1.05
160408A	1.9	< 44.522	...	44.949	44.25	9.32	3.57	-8.767	14.13	...	0.49	0.62
160410A	1.7177	44.897	42.843	45.865	45.166	...	...	...	...	...	...	...
160411A	0.82	< 43.444	...	44.565	43.866	8.87	1.09	-8.833	1.4	...	0.68	0.67
160525B	0.64	< 43.509	...	43.218	42.519	8.04	1.38	-7.9	5.5	...	0.14	...
160601A	0.64	43.423	42.475	44.472	43.773	...	...	...	1.38	...	...	...
160624A	0.484	< 44.396	...	44.837	44.138	9.74	1.28	-9.633	9.63	2.37	0.55	1.19
160821B	0.162	41.677	40.853	43.841	43.142	9.24	0.24	-9.86	15.74	4.24	0.01	0.58
160927A	0.64	42.248	41.424	44.549	43.85	...	...	...	...	...	...	...
161001A	0.67	...	...	45.831	45.132	9.73	0.53	-10.006	18.54	...	0.45	0.78
161104A	0.793	...	...	43.792	43.093	10.23	0.06	-11.452	1.66	...	0.08	2.26
170127B	2.21	< 44.675	...	45.107	44.408	9.51	10.25	-8.499	10.37	...	0.58	0.31
170428A	0.453	42.43	41.606	44.561	43.862	9.68	0.4	-10.078	7.72	...	...	5.14
170728A	1.493	...	...	45.735	45.037	10.09	79.83	-8.188	32.25	...	1.72	0.16
170728B	1.272	44.242	43.418	46.995	46.296	9.87	10.88	-8.833	8.4	...	0.42	0.41
170817	0.01	...	...	...	...	10.61	0.02	-12.309	2.125	0.57	0.03	10.42
180402A	0.64	< 43.18	...	44.428	43.729	...	...	...	...	...	...	...
180418A	1.56	45.108	43.146	45.982	45.283	9.83	13.0	-8.716	1.3	...	1.3	0.56
180618A	0.52	43.772	42.948	44.683	43.984	8.81	1.87	-8.538	9.7	...	0.32	0.35
180727A	1.95	< 46.184	...	45.391	44.692	9.23	3.07	-8.743	2.56	...	0.68	0.54

Table B2 *continued*

**Table B2** (*continued*)

GRB	z	$\log(L_{C,\text{opt}})$	$\log(\sigma_{L_{C,\text{opt}}})$	$\log(L_{C,\text{X}})$	$\log(\sigma_{L_{C,\text{X}}})$	$\log(M_*/M_\odot)$	SFR	$\log(\text{sSFR})$	$\delta R_{\text{phys}}$	$\delta R_{\text{norm}}$	$A_V, \text{host}$	$t_m$
		[erg/s]	[erg/s]	[erg/s]	[erg/s]		[ $M_\odot \text{ yr}^{-1}$ ]	[yr $^{-1}$ ]	[kpc]	[ $r_e$ ]	[mag]	[Gyr]
180805B	0.661	...	...	44.489	43.79	9.34	1.53	-9.155	24.3	...	0.28	0.50
181123B	1.754	43.581	42.757	44.951	44.252	9.9	11.72	-8.831	5.08	...	0.36	0.63
191031D	1.93	< 44.783	...	44.751	44.053	10.38	36.14	-8.822	13.08	...	1.41	0.8
200219A	0.48	< 44.757	...	43.012	42.313	10.74	9.91	-9.744	8.3	...	0.96	3.52
200411A	0.82	...	...	45.364	44.665	10.23	27.35	-8.793	37.66	...	1.52	0.62
200522A	0.554	< 43.471	...	44.694	43.995	9.66	2.23	-9.312	0.93	0.24	0.01	0.58
200907B	0.56	...	...	44.006	43.307	9.35	1.32	-9.229	2.41	...	0.59	0.89
201006A	0.64	...	...	43.793	43.094	...	...	...	...	...	...	...
201221D	1.055	43.455	42.631	43.299	42.6	9.36	2.36	-8.987	29.35	...	0.17	0.27
210323A	0.733	42.916	41.714	45.466	44.767	8.77	0.34	-9.239	5.89	...	0.07	0.56
210726A	0.37	< 42.968	...	44.31	43.611	7.84	0.06	-9.062	0.23	...	0.68	1.06
210919A	0.242	< 42.424	...	41.846	41.147	9.87	0.3	-10.393	51.05	...	0.8	1.62
211023B	0.862	45.137	44.313	45.222	44.523	9.65	1.44	-9.492	3.84	...	0.42	1.72
211106A	0.64	< 42.5	...	45.461	44.762	...	...	...	0.79	0.49	...	...
211211A	0.0763	42.32	41.49	44.453	43.754	8.84	0.07	-9.995	7.92	3.2	0.05	2.53
220412B	0.64	< 44.447	...	...	...	...	...	...	...	...	...	...
221120A	0.64	< 43.855	...	...	...	...	...	...	...	...	...	...
230205A	0.429	...	...	45.069	44.37	...	...	...	...	...	...	...
230217A	0.64	...	...	45.715	45.016	...	...	...	...	...	...	...
230228A	0.64	< 44.06	...	44.822	44.123	...	...	...	...	...	...	...
230307A	0.065	44.51	43.69	43.81	43.11	9.66	0.09	-10.71	38.9	12.1	0.27	5.5
231117A	0.257	43.543	41.929	44.45	43.75	9.16	0.39	-9.57	2.0	...	0.82	1.62

NOTE—Environmental properties were taken from the Broadband Repository for Investigating Gamma-ray burst Host Traits (BRIGHT; Fong et al. 2022; Nugent et al. 2022) and from Levan et al. (2024); Schroeder et al. (2025); Nugent et al. (2025)